Palaeogeography, Palaeoclimatology, Palaeoecology 629 (2023) 111778

Contents lists available at ScienceDirect

Palaeogeography, Palaeoclimatology, Palaeoecology

journal homepage: www.elsevier.com/locate/palaeo

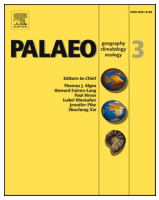

Calcareous nannofossils across the Eocene-Oligocene transition: Preservation signals and biostratigraphic remarks from ODP Site 1209 (NW Pacific, Shatsky Rise) and IODP Hole U1411B (NW Atlantic Ocean, Newfoundland Ridge)

Allyson Viganò [a,*], Thomas Westerhold [b], Paul R. Bown [c], Tom Dunkley Jones [d], Claudia Agnini [a]

[a] Dipartimento di Geoscienze, Università di Padova, Via Gradenigo 6, 35131 Padova, Italy
[b] Center for Marine Environmental Sciences (MARUM), University of Bremen, Leobener Strasse, 28359 Bremen, Germany
[c] Department of Earth Sciences, University College London, Gower Street, WC1E 6BT London, United Kingdom
[d] School of Geography, Earth and Environmental Sciences Birmingham, Edgbaston, B15 2TT Birmingham, United Kingdom

ARTICLE INFO

Editor: Prof. M Elliot

Keywords:
Calcareous nannofossils
EOT
Preservation
Biostratigraphy
IODP Hole U1411B
ODP Site 1209

ABSTRACT

This work provides a detailed biostratigraphic correlation through the Eocene-Oligocene Transition (EOT), based on an integrated stratigraphic approach and the study of calcareous nannofossils, between two disparate sites, one in the NW Atlantic (IODP Hole U1411B) and one in the NW Pacific (ODP Site 1209).

The precise site-to-site correlation provided by these data allows for a comparison of carbonate preservation across the EOT including identification of the main post-depositional processes that impact the calcareous nannofossil ooze at Site 1209. The main aim of this work is to understand the extent to which the bulk $\delta^{18}O$ and $\delta^{13}C$ records and their sources (mainly calcareous nannofossils) are altered by diagenesis. Our detailed SEM study highlights some differences before, during and after the EOT, suggesting local diagenetic dynamics.

At Site 1209, a distinctive change, both in nannofossil assemblage composition and preservation state, is observed from the pre-EOT phase to the Late Eocene Event (LEE), with a shift in the dominant process from dissolution to recrystallisation. Surprisingly, despite the overall poor preservation, only the interval between 141 and 142.4 (adj. rmcd) was compromised in term of isotopic values and assemblage diversity and abundance. This interval, recorded in the upper Eocene, was characterized by severe dissolution, concomitant with deposition of secondary calcite on solution-resistant forms. Diagenetic processes have strongly biased the $\delta^{18}O$ isotopic signal, resulting in a positive oxygen isotope anomaly through the upper Eocene that is difficult to reconcile with other published trends. For the remaining time intervals, diagenesis seems not to have altered the bulk $\delta^{18}O$ profile, which closely resembles that of other sites across the world, and is particularly consistent with other data from the Pacific Ocean. In summary, the impact of diagenesis on nannofossil preservation even if clearly visible both in SEM and optical microscope observations does not always cause a pervasive alteration of the primary isotopic signal and can instead provide important clues on local depositional dynamics.

1. Introduction

The global cooling trend that started at the end of the Early Eocene Climatic Optimum (EECO; ~50 Ma) culminated at ~34 Ma in the Eocene-Oligocene transition (EOT), with the rapid growth of the Antarctica ice sheet (Zachos et al., 2001, 2008; Coxall and Pearson, 2007; Westerhold et al., 2020). The effects of the EOT on calcareous nannoplankton have been documented at different sites worldwide, providing important paleoenvironmental insight and biostratigraphic implications for this fundamental event (Persico and Villa, 2004; Dunkley Jones et al., 2008; Villa et al., 2008, 2014, 2021; Bordiga et al., 2015; Jones et al., 2019). The hallmark of this event is globally recognizable, often represented by a two-stepped positive excursion in the oxygen ($\delta^{18}O$) and/or carbon ($\delta^{13}C$) isotopic values of marine carbonates that are hereafter referred as to Step 1 and Step 2 (or EOIS - i.e. “earliest Oligocene oxygen isotope step”) (Coxall and Pearson, 2007;

* Corresponding author.
E-mail address: allyson.vigano@unipd.it (A. Viganò).

https://doi.org/10.1016/j.palaeo.2023.111778
Received 28 April 2023; Received in revised form 13 August 2023; Accepted 15 August 2023
Available online 22 August 2023

Hutchinson et al., 2021). During this time, in the Pacific Ocean, there is also a > 1 km deepening of the calcite compensation depth (CCD) associated with the rapid stepwise increase in the benthic oxygen stable isotope record (Coxall et al., 2005; Pälike et al., 2012; Westerhold et al., 2014). The Early Oligocene Glacial Maximum (EOGM) is associated with a prominent $\delta^{18}O$ maximum (Zachos et al., 1996; Liu et al., 2004) that corresponds to an extended glaciation during the earliest Oligocene (Miller et al., 1991; Hutchinson et al., 2021). The EOGM appears to have coincided with a cold-eutrophic phase in marine environments that persisted for ca. 500–700 kyr, which is supported by observed changes in calcareous nannofossil assemblages, characterized by increased abundances of taxa better adapted to increased nutrient availability and a cooler regime (e.g., Dunkley Jones et al., 2008; Fioroni et al., 2015; Villa et al., 2014, 2021; Jones et al., 2019; Viganò et al., 2023).

Although calcareous nannofossil sensitivity to the Antarctic glaciation is now well-documented (see references above), questions remain as

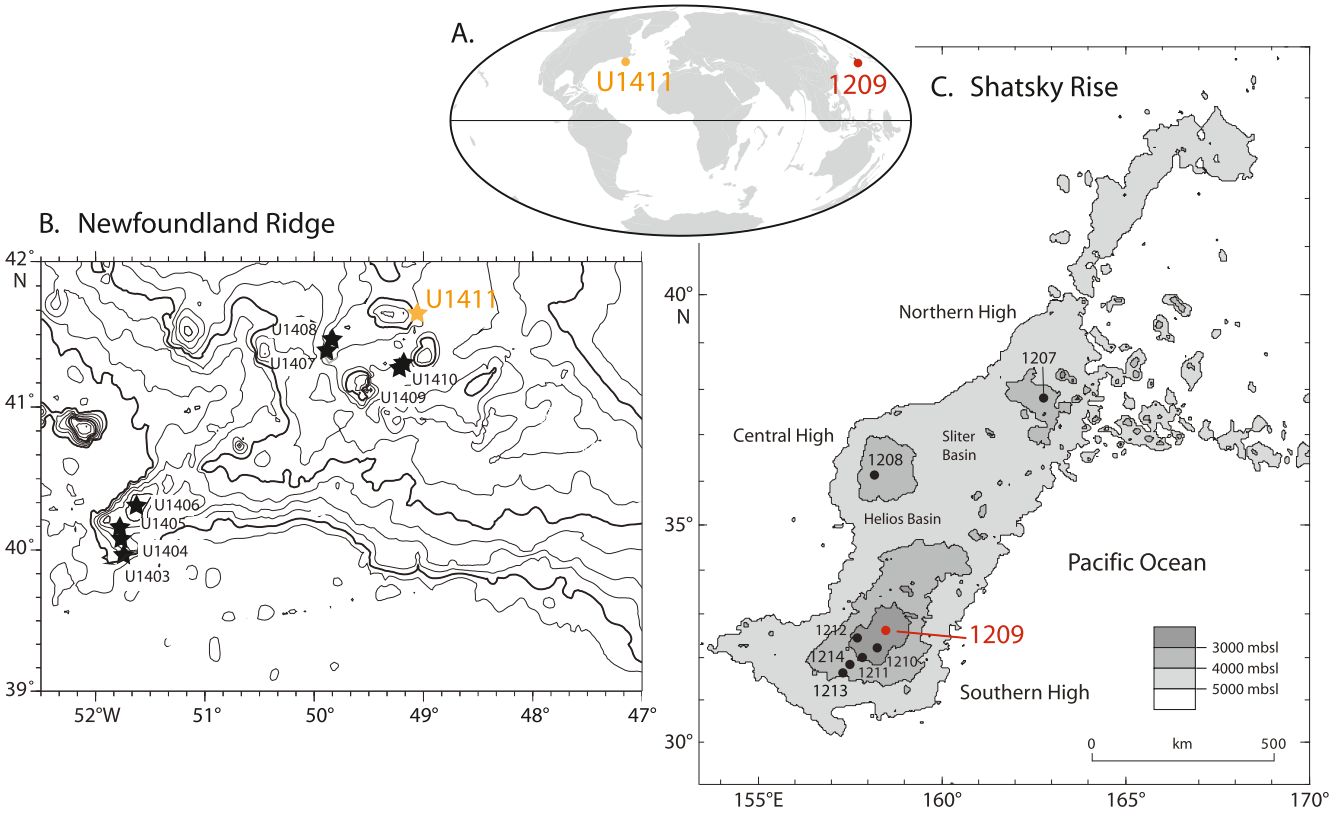

Fig. 1. A. Present-day locations of the study sites, Site U1411 (yellow circle) and Site 1209 (red circle), respectively on Newfoundland Ridge (NW Atlantic) and Shatsky Rise (NW Pacific). B, C. Bathymetric maps showing the location of IODP/ODP sites drilled on Newfoundland Ridge (modified after Norris et al., 2014) and Shatsky Rise (modified after Bown, 2005). (For interpretation of the references to colour in this figure legend, the reader is referred to the web version of this article.)

Table 1
Age and mid-depth of selected calcareous nannofossil biohorizons from Hole U1411B and from Site 1209. Ages are from Agnini et al. (2014) recalibrated to GTS20 (Gradstein et al., 2020). *Points chosen as tie points. #Ages for Hole U1411B calibrated with respect to magnetostratigraphy (Norris et al., 2014). @Ages for Hole U1411B given with respect to magnetostratigraphic Chron boundaries (Norris et al., 2014) and calcareous nannofossil tie-points (excluded the Top of *E. formosa*). $Ages for Site 1209 are calibrated with respect to calcareous nannofossil and oxygen stable datums. NA = not available; NI = not identified. T = top; Tc = top common; Bc = base common and continuous; B = base; Bi = base of acme increase. The age reported for T EOIS is from Hutchinson et al. (2021) recalibrated to GTS20.

Events	Hole U1411B		Site 1209		Hole U1411B		Site 1209	Age (Ma)
	Mid-depth (mbsf)	Error (± m)	Mid-depth (adj. rmcd)	Error (± m)	Age (Ma) U1411#	Age (Ma) U1411@	Age (Ma) 1209$	GTS20
T *R. umbilicus* *	99.95	2.25	126.68	0.13	32.25	31.98	31.98	**31.98**
T *I. recurvus*	103.78	1.58	128.05	0.25	32.38	32.14	32.19	
Tc *C. subdistichus* gr.	117.02	1.64	130.98	0.13	32.82	32.71	32.62	
Base Chron C12r *	128.79	0.73	NA	NA	33.214	33.214	33.214	**33.214**
T *E. formosa* *	130.80	2.79	132.83	0.08	33.28	33.28	32.90	**32.90**
Tc *I. recurvus*	130.80	2.79	133.33	0.13	33.28	33.28	33.01	
B *S. akropodus*	133.85	0.27	134.20	0.25	33.38	33.38	33.19	
T EOIS *	NA	NA	136.45	NI	NA	NA	33.67	**33.67**
Base Chron C13n *	144.15	0.05	NA	NA	33.726	33.726	33.214	**33.726**
Bi *C. subdistichus* gr.	154.71	1.20	137.78	0.22	34.23	34.04	33.98	
Bc *C. subdistichus* gr.	172.39	0.02	140.23	0.13	35.07	35.02	34.56	
T *Hantkenina*	157.46	0.75	140.36	NI	34.36	34.13	34.59	**33.90**
T *D. saipanensis* *	167.87	1.27	139.73	0.13	34.86	34.44	34.44	**34.44**
T *D. barbadiensis*	170.58	1.44	139.73	0.13	34.99	34.76	34.44	**34.76**
B *S. predistentus*	172.39	0.02	140.68	0.08	35.07	35.02	34.66	
Base Chron C13r *	172.98	0.08	NA	NA	35.102	35.102	33.214	**35.102**
T *C. reticulatum* *	177.74	0.31	NI	NI	35.33	35.31	NI	**35.31**

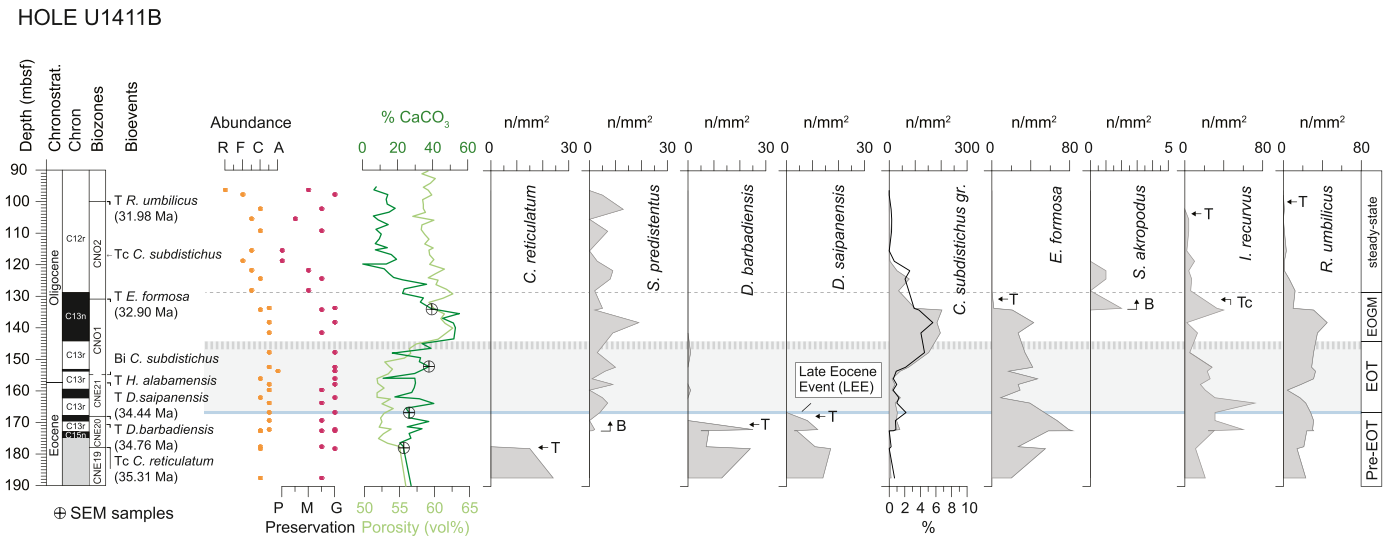

Fig. 2. Semi-quantitative abundance patterns (n/mm^2) of selected taxa from IODP Hole U1411B are plotted against depth (mbsf), chronostratigraphy, magnetostratigraphy (Norris et al., 2014), CN biozone (Agnini et al., 2014), abundance, and preservation. Nannofossil data are also compared to carbonate content (wt%) and porosity (vol%) (from Norris et al., 2014). Biochronology after Agnini et al. (2014) recalibrated to GTS20 (Gradstein et al., 2020). The grey band highlights the EOT (base coinciding with the Top of *D. saipanensis*), while the dashed grey line in the upper part is inferred to denote Step 2 (or EOIS). The light blue line indicates the Late Eocene Event (LEE) (see text for discussion). Four intervals are reported: Pre-EOT, EOT, EOGM and steady-state. (For interpretation of the references to colour in this figure legend, the reader is referred to the web version of this article.)

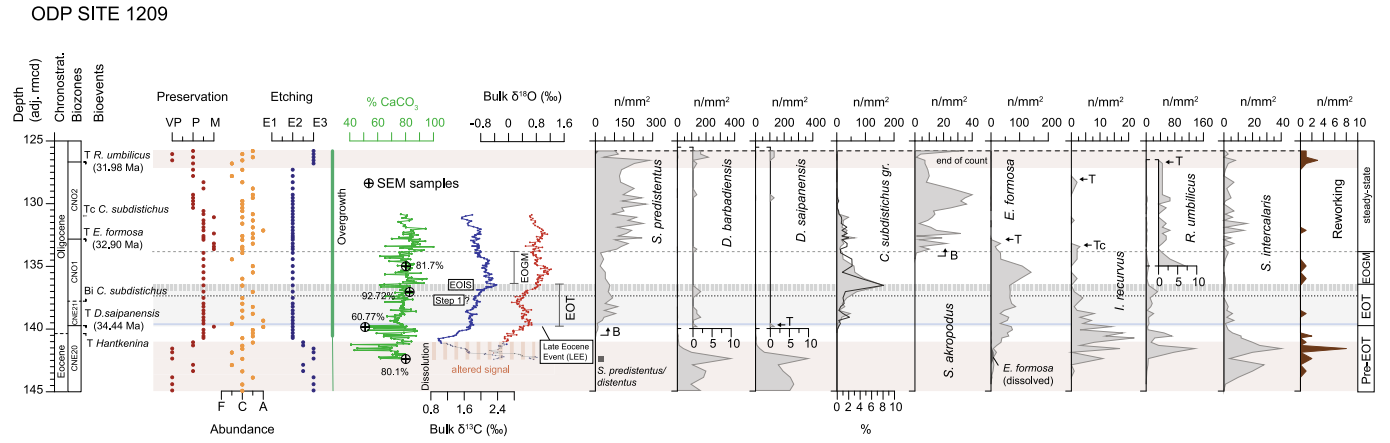

Fig. 3. Semi-quantitative abundance patterns (n/mm^2) of selected taxa from ODP Site 1209 are plotted against depth (adj. rmcd), chronostratigraphy, CN biozone (Agnini et al., 2014), preservation, abundance, etching, geochemistry (stable O, C isotopes and % $CaCO_3$). The grey band highlights the EOT (base coinciding with the Top of *D. saipanensis*), while the dashed grey line in the upper part is inferred to denote Step 2 (or EOIS). Biochronology after Agnini et al. (2014) recalibrated to GTS20 (Gradstein et al., 2020). The light blue line indicates the Late Eocene Event (LEE) (see text for discussion). The dashed pink bar highlights the altered geochemical signature linked to the dissolution interval. Reworking corresponds to interval of higher dissolution, as highlighted by the pink bar. (For interpretation of the references to colour in this figure legend, the reader is referred to the web version of this article.)

to the influence of changes in nannofossil preservation state – driven by shifting oceanic carbonate chemistry – on both assemblage records and bulk pelagic carbonate geochemical records.

Global-scale climate and environmental perturbations (e.g., OAEs – Oceanic Anoxic Events, the K/Pg boundary – Cretaceous-Paleogene boundary, PETM – Paleocene-Eocene Thermal Maximum, and EOT – Eocene-Oligocene Transition) are often associated with large anomalies in the marine carbon cycle, most commonly manifested as major changes in carbonate saturation state favoring either strongly enhanced dissolution or improved preservation of deep ocean calcium carbonate (e.g., Schlanger and Jenkyns, 1976; Jenkyns, 1980; Coxall et al., 2006; Agnini et al., 2007; Dunkley Jones et al., 2008; Pearson et al., 2008; Raffi and De Bernardi, 2008; Birch et al., 2016). Most of our understanding of oceanic paleoenvironmental change is derived from calcareous microfossils, with the quality of information extracted from these being strongly dependent on preservation state (e.g., Pearson et al., 2001; Bown et al., 2008). Understanding the filter imposed by changing diagenetic conditions on primary ecological and geochemical signals is not straightforward. Preservational filters for calcareous nannofossils are primarily the dissolution and/or overgrowth of specimens. Dissolution preferentially obliterates the more delicate structures and can completely remove small/delicate taxa from pelagic carbonates (Bown et al., 2008), with the extent of dissolution strongly coupled to the depth of the site of deposition relative to the carbonate and aragonite compensation depth (CCD, ACD) and lysocline (Honjo, 1976), as well as sedimentary organic carbon and clay content (Bown and Dunkley Jones, 2006). Overgrowth with secondary calcite generally affects the larger crystallites of coccoliths and nannoliths and is thought to be dominated by processes in sediment pore fluids (Staudigel and Swart, 2019; Cisneros-Lazaro et al., 2022). Both, the taxonomic composition of

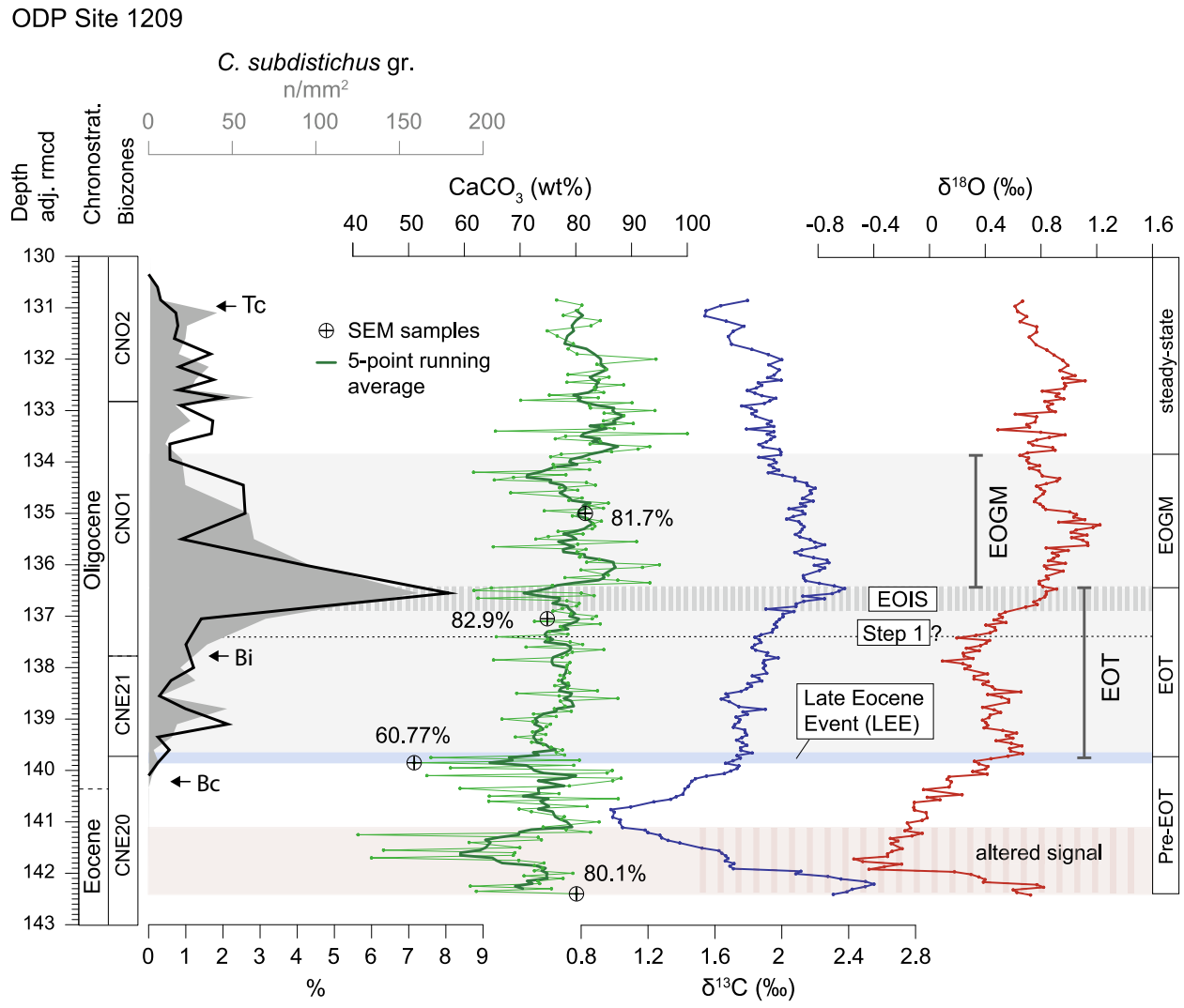

Fig. 4. Profile of carbonate content (wt%), stable oxygen and carbon isotopes (‰ VPDB), *C. subdistichus* gr. abundance (n/mm^2 and %) plotted against chronostratigraphy, CN biozone (Agnini et al., 2014) and the four main intervals: pre-EOT, EOT, EOGM and steady-state at Site 1209. The altered geochemical signature is highlighted by the pink bar. The main oxygen stable isotopic events are reported: Late Eocene Event (LEE), EOT (Step 1 and EOIS) and EOGM. Bi = base of increase; Bc = base common and continuous; Tc = top common and continuous refers to *C. subdistichus* gr. (n/mm^2) plot. (For interpretation of the references to colour in this figure legend, the reader is referred to the web version of this article.)

assemblages and accurate species identification can be strongly impacted by these taphonomic and diagenetic processes (Roth and Thierstein, 1972; Roth, 1978; Bown et al., 2008). Our study is designed to survey different nannofossil preservation states in four well defined and documented phases across the EOT. We also consider whether the bulk $\delta^{18}O$ and $\delta^{13}C$ records are biased by carbonate diagenesis with preferential recrystallization or dissolution of nannofossils at or beneath the seafloor.

To investigate the effective role of preservation on taxonomic composition, we decide to compare two sites (ODP Site 1209, Bralower et al., 2002b; IODP Site U1411, Norris et al., 2014) with different preservation states and lithologies. Another goal of this work is to comprehensively discuss the relationship between biostratigraphic data and assemblage components, changes in sea-water carbonate chemistry, sedimentary carbonate content and porosity. To achieve these goals, we first provide an estimate of the abundances and preservation of nannofossils at Hole U1411B and ODP Site U1209 by means of light transmitted microscope (LM) and scanning electron microscope (SEM) analyses on the assemblage.

2. Materials and methods

2.1. Hole U1411B and Site 1209

The present study is based on cores that span the EOT, recovered during IODP Exp. 342 (Norris et al., 2012, 2014) at Hole U1411B (SE Newfoundland Ridge; NW Atlantic Ocean) and ODP Leg 198 (Bralower et al., 2002a) at Site 1209 (Shatsky Rise; NW Pacific) (Fig. 1).

During the drilling of the northwest Atlantic Site U1411 (~3300 m water depth), a 254.5 m-thick sedimentary succession of deep-sea sediment of Pleistocene to late Eocene age was recovered. The sedimentary sequence at Site U1411 consists of three lithostratigraphic units: Unit I (14.45 m of Pleistocene sediments; composed of clayey foraminiferal ooze), Unit II (a 198.23 m-thick succession of early Miocene to late Eocene age; composed of silty clay, clay with nannofossils, silty nannofossil clay, and clayey nannofossil ooze with silt) and Unit III (41.92 m-thick succession of upper Eocene sediments composed by clayey nannofossil chalk and clayey nannofossil chalk with foraminifers) (Norris et al., 2014). Three holes (A, B, C) were drilled at this site, allowing recovery of an expanded clay-rich (~25–50%) supra-CCD succession of sediment drift characterized by faster accumulation rates

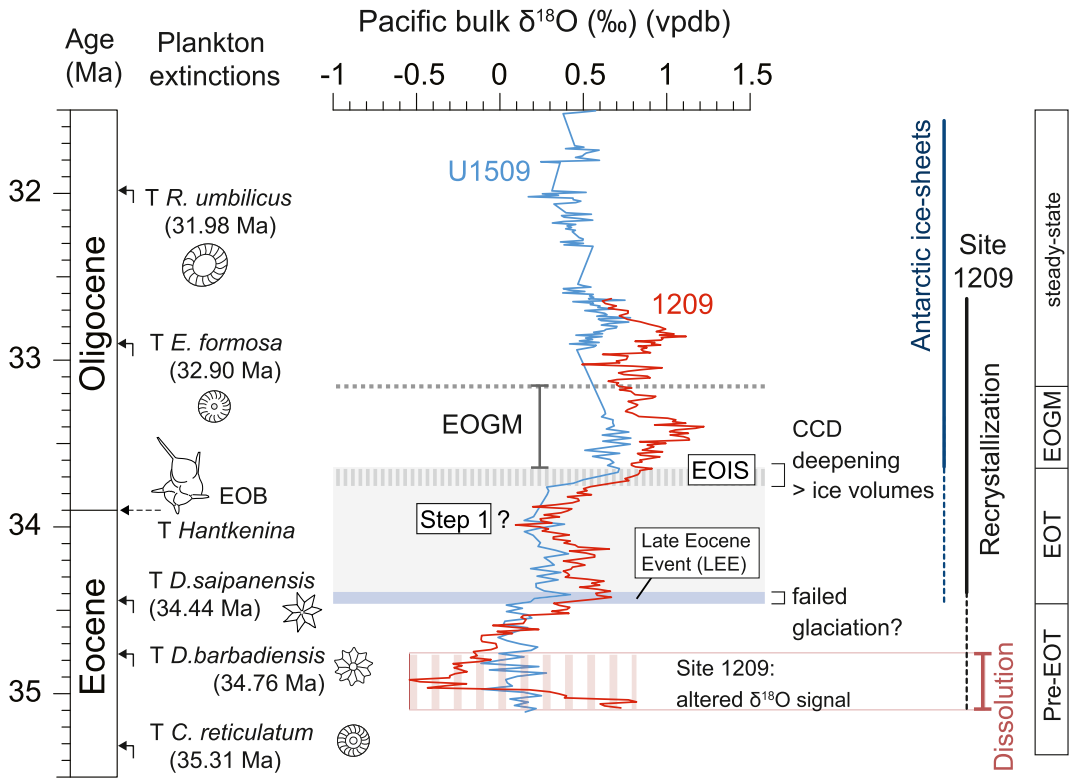

Fig. 5. Pacific Ocean bulk stable oxygen isotopes records (‰ VPDB) from Site 1209 (this work) and Site U1509 (Viganò et al., in prep.). A summary of the main environmental and geochemical events occurring across the E-O transition is also reported, as well as the main plankton extinctions. The dissolution phase is highlighted by a dashed pink bar, corresponding to strongly altered geochemical signature at Site 1209, concomitant to modest recrystallization. Biochronology after Agnini et al. (2014) recalibrated to GTS20 (Gradstein et al., 2020). (For interpretation of the references to colour in this figure legend, the reader is referred to the web version of this article.)

compared to typical deep-sea sediments (Norris et al., 2014). The paleowater depth for the late Eocene - early Oligocene at Site U1411 is estimated to be 2800 m (Newsam, 2017). In this work, we focus our sampling on sediments recovered from Hole U1411B. Upper Eocene sediments are included in lithological Unit II and predominantly consists of clayey nannofossil ooze with increased carbonate content across the EOT.

We analyzed an expanded record of the EOT from core 342-U1411B-22X to core 342-U1411B-11H, spanning 187.35 to 96.25 mbsf (meter below sea floor or CSF-A, Core depth below Sea Floor-A).

The second site, ODP Site 1209, situated on the Southern High of Shatsky Rise at middle bathyal water depth, has been chosen for its geographical location. Three holes (Holes A, B, C) were drilled at this site, whose cores have been aligned and placed into a composite adj. rmcd (adjusted revised meters composite depth) scale (Westerhold and Röhl, 2006). Sediments from Site 1209 are open ocean pelagic and mainly consist of nannofossil ooze and nannofossil ooze with clay.

The EOT record is characterized by a gradual colour change from a light brown nannofossil ooze with clay to a light grey nannofossil ooze (Bralower et al., 2002b). This lithological change corresponds to an increase in carbonate content that occurs in the early Oligocene and indicates a deepening of the CCD (Pälike et al., 2012).

At present, Site 1209 is situated at 2387 m water depth, well above both the lysocline and the CCD, which are at 3500 and 4100 m, respectively (Bralower et al., 2002b). During the EOT, the inferred paleodepth of this site was relatively shallower, at approximately ~2000 m (Bralower et al., 2002a). The studied section spans the late Eocene to early Oligocene and ranges from 144.95 to 125.80 adj. rmcd (from 1209B-15H-3W, 95 cm to 1209A-13H-2W, 87 cm), equivalent to nannofossil biozones CNE20 to CNO2 (Agnini et al., 2014).

2.2. Calcareous nannofossil assemblage counts

Micropaleontological analyses were performed on a total of 88 samples, recovered from Site 1209 (58 samples) and Hole U1411B (30 samples). Calcareous nannofossils were semi-quantitatively investigated in standard smear-slides (Bown and Young, 1998), using the light microscope (LM), under cross-polarized (XPL) and phase contrast light (PC) at 1250× magnification. The abundance of selected taxa was determined by counting the number of the observed specimens in a predetermined area of 1 mm^2 (Backman and Shackleton, 1983) and then plotted versus depth. Biohorizon nomenclature follows that given by Agnini et al. (2014): Base (B), Base common (Bc), Top (T) and Top common (Tc).

Preservation of the nannofossils varied significantly because of two different processes, etching and calcite overgrowth. Preliminary observations to estimate the preservation state of the samples were performed using a transmitted light microscope. The abundance and etching levels were used to estimate the general preservation state. Preservation was defined as follows (Norris et al., 2014):

G = good (slight or no sign of dissolution and/or overgrowth; principal morphological characteristics unaltered; specimens identifiable to the species level).

M = moderate (some evidence of etching and/or overgrowth; primary morphostructures slightly altered; most specimens identifiable to the species level).

P = poor (severe etching and/or overgrowth; morphological characteristics largely destroyed; fragmentation; specimens could not be identified at the species and/or generic level).

VP = very poor (extreme etching and/or overgrowth; distinctive morphological features unrecognizable; fragmentation; presence of only

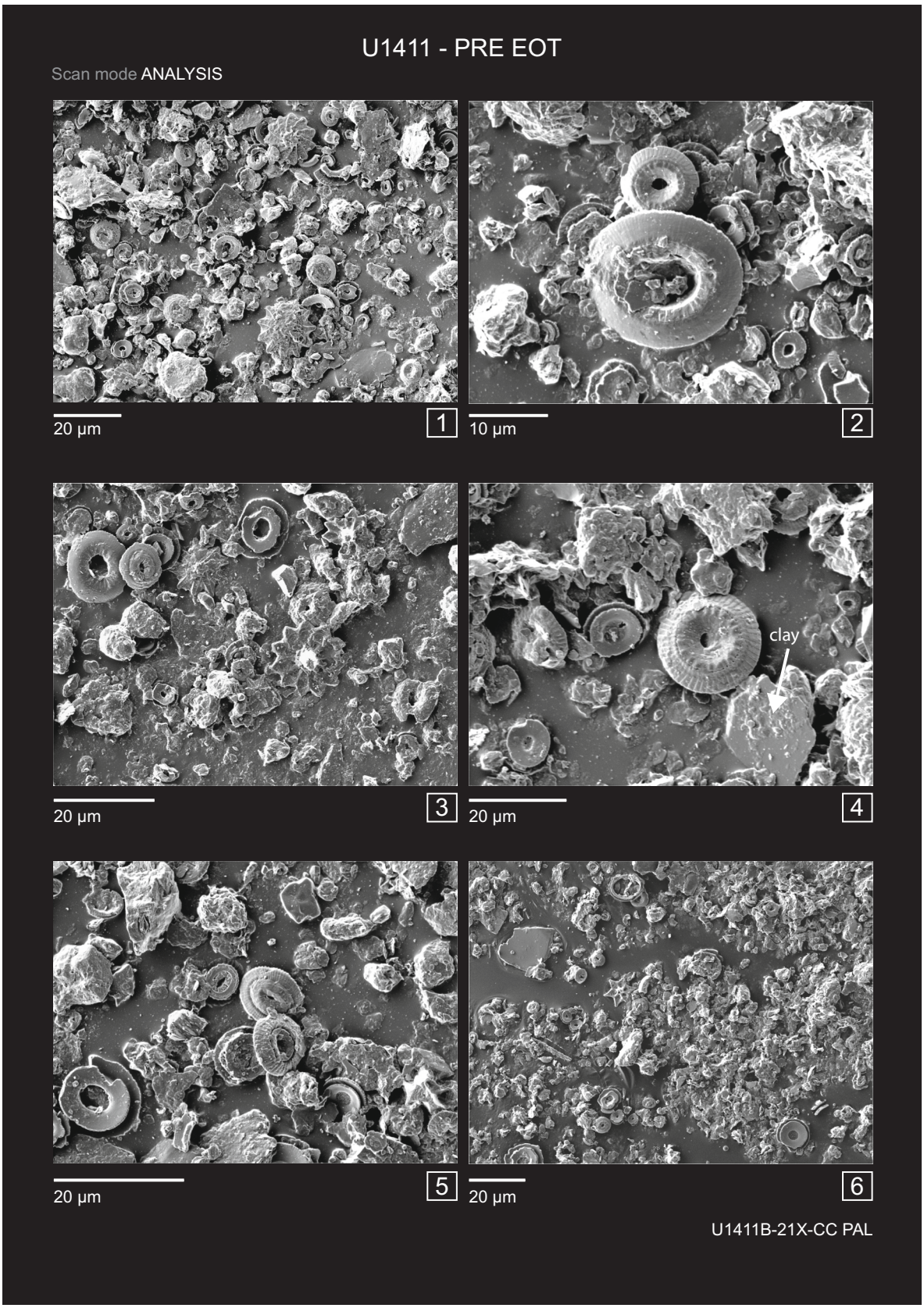

Fig. 6. Scanning electron photomicrographs showing the preservation of PRE-EOT calcareous nannofossils from Site U1411 (sample U1411-21X-CC, 25-33 cm). Insets:

1–6 Analysis scan mode micrographs showing the assemblage constituents.

7–8 ***Discoaster barbadiensis*** shown in UH resolution (7) and analysis scan mode (8).

9 Another specimen of ***Discoaster barbadiensis*** with no evidence for diagenetic overgrowth on the rays. The UH resolution micrographs (7, 9) highlight the

extremely good preservation of the specimens.
10–12 Analysis scan mode (10) and UH resolution scan mode (11-12) images of ***Discoaster saipanensis***.
13–15 Specimens of ***Discoaster robustus*** with 11 (13–14) and 10 rays (15), respectively.
16 Distal view of ***Coccolithus pelagicus*** with intact elements.
17 Distal view of ***Clausicoccus fenestratus*** with its highly perforated central area.
18 ***Cribrocentrum reticulatum*** (<12 μm), proximal view. The narrow central area is spanned by a robust and visible grid.
19–20 UH resolution (19) and analysis scan mode (20) images of ***Chiasmolithus*** **cf.** ***C. altus*** in distal view. The micrograph shows the cross bars with their complex construction.
21 ***Discoaster saipanensis*** showing a highly-defined central stem and distinct radial sutural ridges and depressions.
22 Distal view of ***Chiasmolithus oamaruensis***.
23 ***Ericsonia formosa*** distal view.
24 Proximal view of reticulofenestrids. The left specimen (***Reticulofenetra daviesii***) exhibits a delicate and well-preserved net in the central area.

few highly resistant species; difficulties in identifying specimens also at the genus level).

We also attempted to evaluate the degree of etching following Roth (1983) using three categories:

E1 = slight etching; subtle central area structures are affected by dissolution but are generally still visible.

E2 = moderate etching; dissolution of delicate central structures in many specimens; some isolated shields with irregular outlines present.

E3 = strong dissolution; only dissolution-resistant species are present; abundant coccoliths fragments.

2.3. Stable isotopes and carbonate content analysis

Geochemical analyses ($CaCO_3$ wt%, C and O stable isotopes) were carried out on a total of 206 bulk samples from ODP Site 1209. Samples were analyzed every 5 cm, ranging from 142.40 adj. rmcd (sample 1209C-4H-3W, 93 cm) to 130.85 adj. rmcd (sample 1209C-3H-2W, 70 cm). All results are given in standard delta notation (‰) with Vienna Pee Dee Belemnite (VPDB) as the reference standard. Analyses were carried out at the Department of Geosciences (University of Padova) using a Delta V Advance Isotopic Ratio Mass Spectrometer equipped with a Gas Bench II device. A known mass (~250 μg) was placed into a headspace vial and flushed with helium. To each sample, 10 mL of 100% phosphoric acid was added and allowed to react. Two standards, Carrara marble Maq 1 ($\delta^{13}C = 2.58‰$; $\delta^{18}O = -1.15‰$VPDB) and marble Gr1 ($\delta^{13}C = 0.68‰$; $\delta^{18}O = -10.44‰$ VPDB) were used for instrument calibration and quality assurance and repeated with precisions better than 0.06‰ for $\delta^{13}C$ and better than 0.09‰ for $\delta^{18}O$ during sample runs. The amount of $CaCO_3$ was calculated from the beam height (Spofforth et al., 2010) of the CO_2 liberated during isotope mass spectrometer measurements.

2.4. Scanning electron microscopy (SEM)

SEM investigations allow an evaluation of the preservation quality of coccoliths, which includes the description of any evidence of diagenetic alteration (e.g., etching, overgrowth). Analyses on the preservation and composition of the assemblages were performed at the Department of Geosciences (University of Padova) using a Tescan Solaris Scanning Electron Microscope (SEM) on both processed and unprocessed samples.

Processed samples were treated as follows: a small amount (~5 mg) of sediment was suspended in distilled water (1.5 mL) and centrifuged using a Rotofix 32A for 2 min at 2000 rpm. The suspension was then placed in a rotating plate (Heidolph Unimax 1010) for 10 h (6 speed intensity) to disaggregate clay particles from calcareous nannofossils. The supernatant was poured off, and the residual was treated ultrasonically for 1 min.

This methodology was necessary to reduce the high amount of clay found in the samples recovered from Hole U1411B. Finally, a drop of the intermediate suspension was placed on a sticky carbon tab placed on a 12.5 mm stub and dried in the oven at 30/40 °C for ~20 min. The stubs were then coated with carbon, deposited through a double-tilted vacuum evaporation procedure using the EMITECH K950X sputter coater. The graphite rod evaporation has the advantage of producing an all-round coating layer, with very fine grain size, ideal for high magnification applications. All images were taken under a high-vacuum mode (<0.04 Pa; HighVac) using the In-beam SE detector, with two different scanning modes: 1) the UH-resolution scan mode for ultrahigh-resolution imaging and 2) the analysis scan mode for compositional assemblage analyses. This latter mode has the benefit of increasing the field of view and thus the dynamic survey of the sample. The disadvantage is a lower resolution compared to the UH-resolution scan mode.

3. Results

3.1. Calcareous nannofossils

Biostragraphic studies carried out at Site 1209 and Hole U1411B are based on the biozonation scheme proposed by Agnini et al. (2014). Analyses performed at these sites reveals distinct trends in the semi-quantitative abundance patterns of selected taxa, which include *Clausicoccus subdistichus* gr. (i.e., *C. subdistichus* and *C. fenestratus*), *Discoaster barbadiensis*, *Discoaster saipanensis*, *Ericsonia formosa*, *Isthmolithus recurvus*, *Reticulofenestra umbilicus*, *Cribrocentrum reticulatum*, *Sphenolithus predistentus*, *Sphenolithus akropodus* and *Sphenolithus intercalaris*. The taxonomy of *C. subdistichus* gr. follows the concept of Viganò et al. (2023).

3.1.1. IODP Hole U1411B

Calcareous nannofossil biostratigraphy from Hole U1411B is based on the analysis of core catcher and additional working section half samples. Depth positions and age estimates of the biostratigraphic events are shown in Table 1. In the study samples calcareous nannofossils are common to abundant and the preservation varies from moderate to good. Only a few samples in the upper part of the section were classified as poorly preserved. A succession of bioevents (Fig. 2) is observed from the upper Eocene Zone CNE19 to the Oligocene Zone CNO2 (Agnini et al., 2014). The estimated duration of the study interval is ~4 Myr (top section 31.82 Ma; base section 35.73 Ma). Site U1411 represents one of the best successions for studying this time interval due to the high sedimentation rates and the good magnetostratigraphic signal (Norris et al., 2014). At this site, the Eocene/Oligocene boundary was identified using the Top of *Hantkenina alabamensis* (planktonic foraminiferal) within Chron C13r (157.46 ± 0.75 mbsf; Norris et al., 2014) following the formal definition of the base of the Rupelian Stage (Premoli Silva and Jenkins, 1993). Although there is no isotopic record yet published for Hole U1411B the stratigraphy presented here is robust, being based on a combination of magnetostratigraphy, calcium

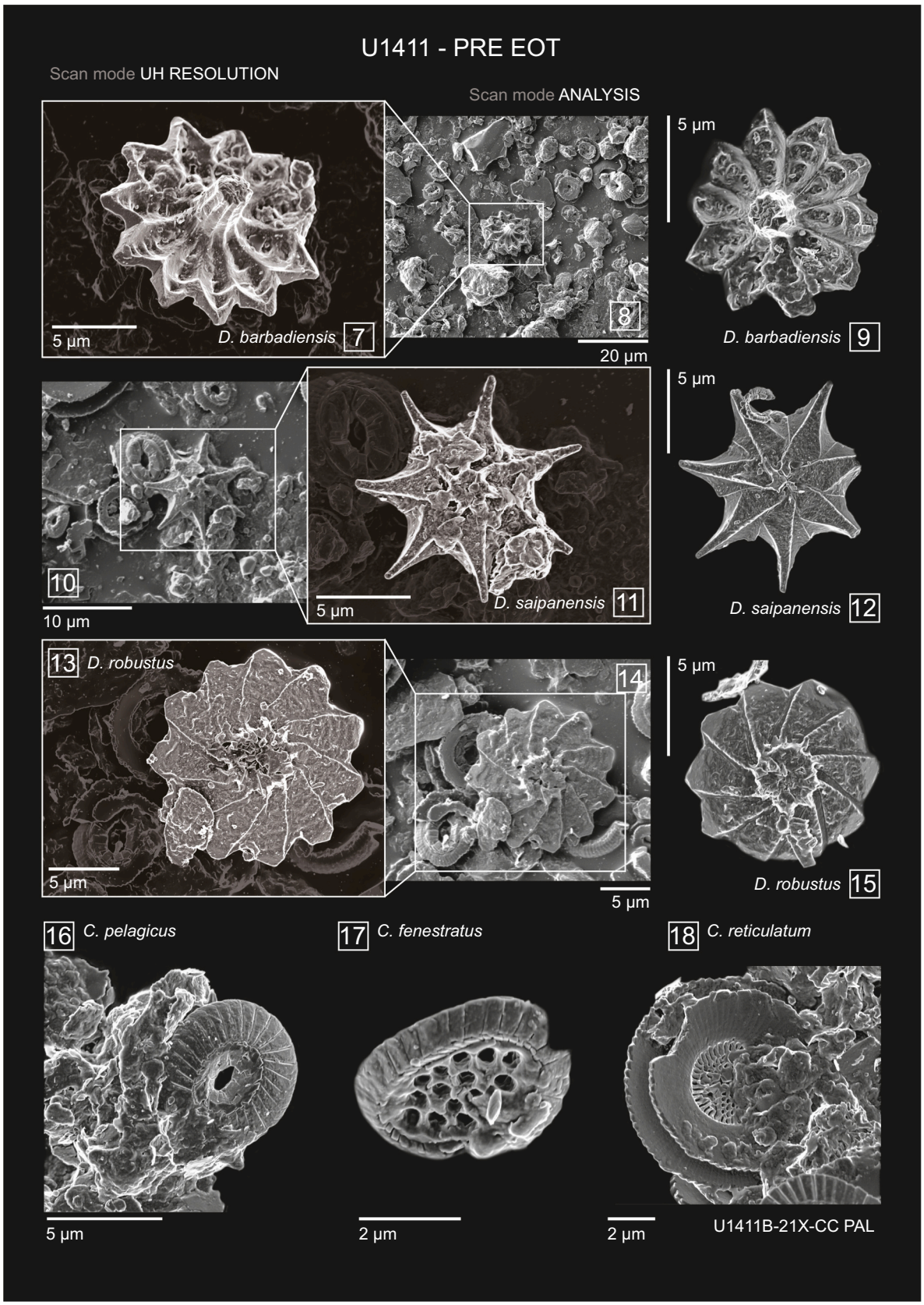

Fig. 6. (*continued*).

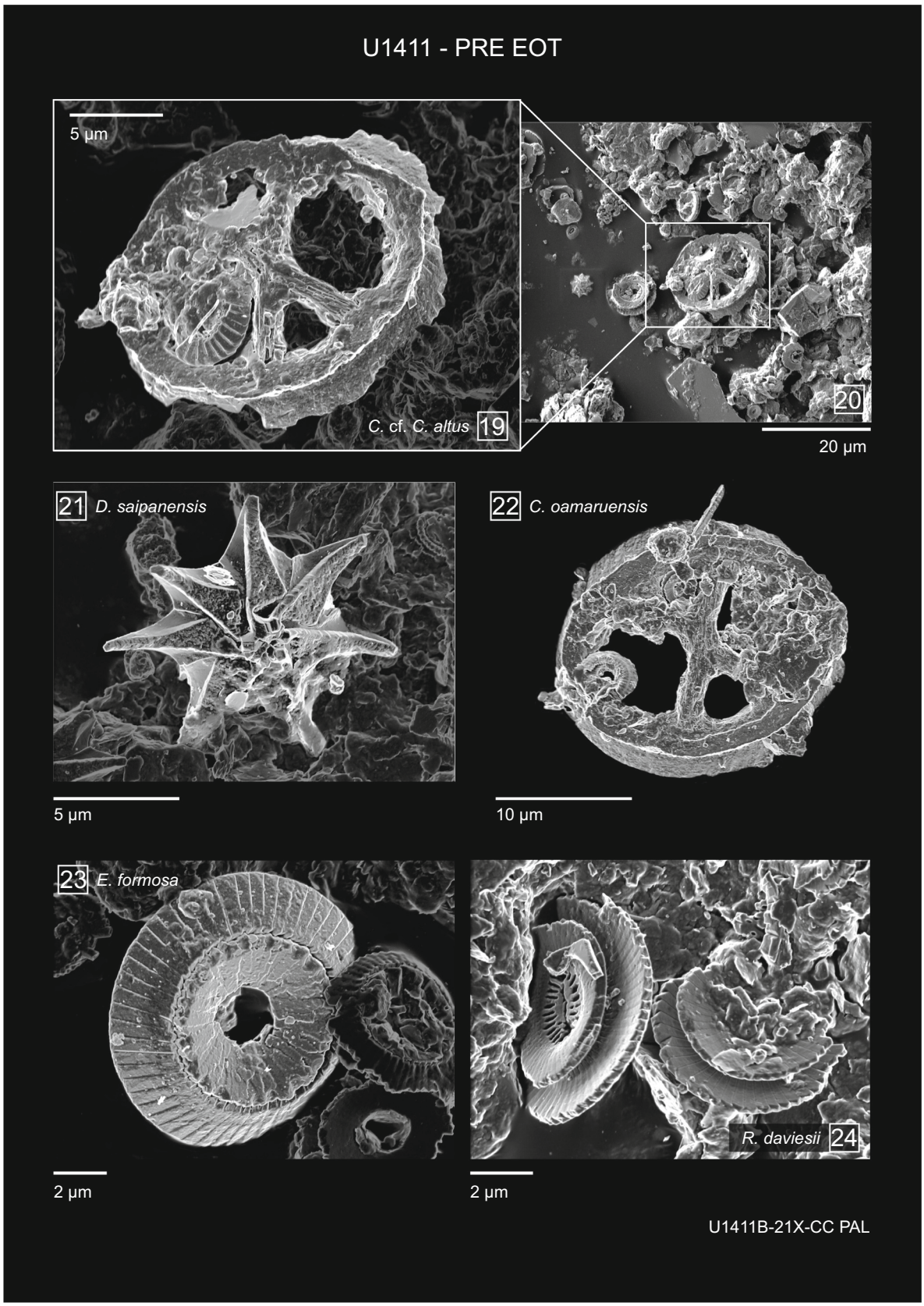

Fig. 6. (*continued*).

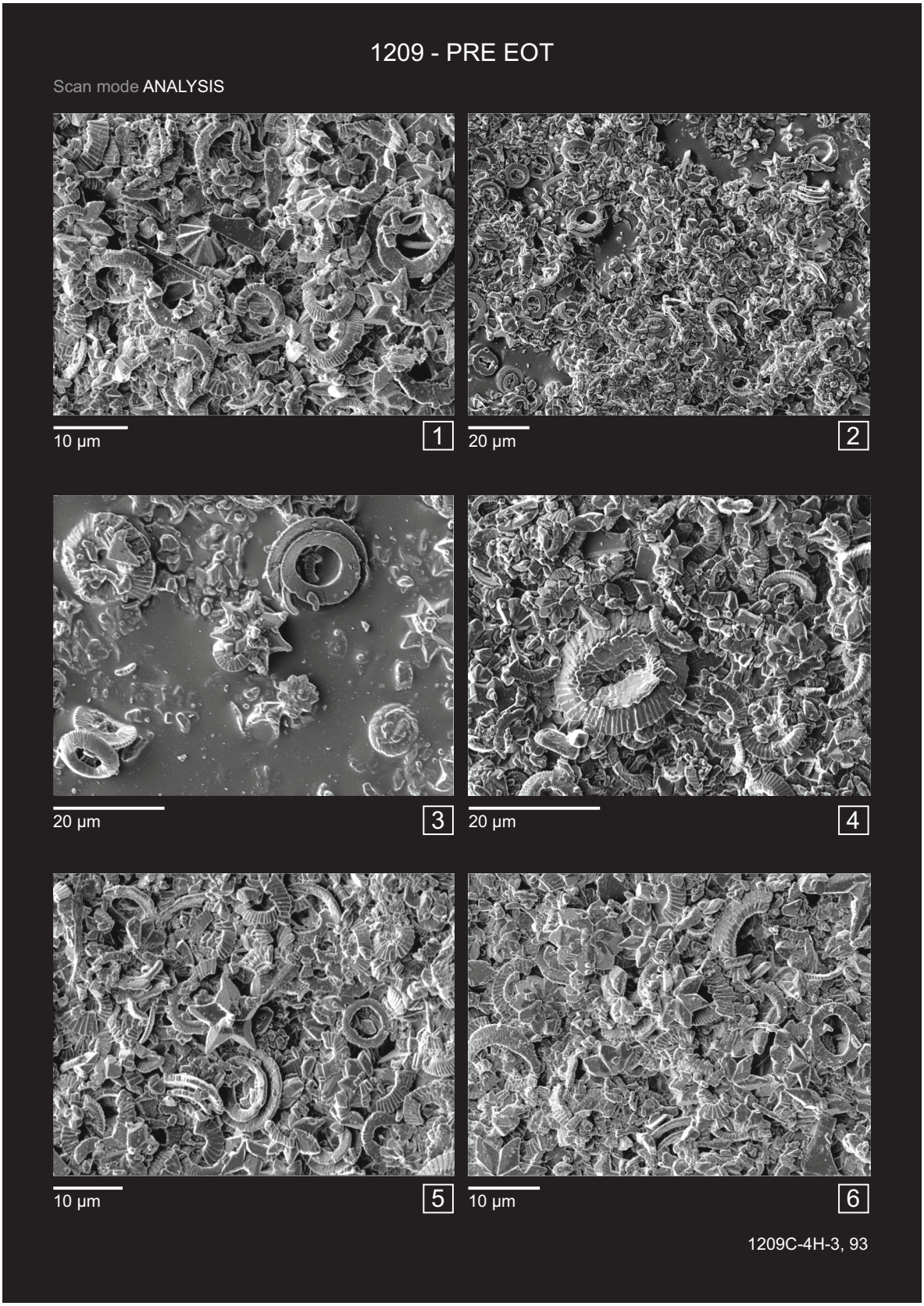

Fig. 7. Scanning electron photomicrographs showing the preservation of PRE-EOT calcareous nannofossils from Site 1209 (sample 1209C-4H-3, 93 cm). Insets:
1–6 Analysis scan mode micrographs showing the assemblage constituents.
7 ***Bramletteius serraculoides*** with severe overgrowth along the c-axis.
8–9 ***Dictyococcites bisectus***, one of the most dissolution-resistant species at the E-O transition (8), here displays blocky accretions in its central plug due to secondary calcite deposition (9).

10 ***Discoaster saipanensis*** showing slight overgrowth.
11 ***Discoaster barbadiensis*** which has accreted a large amount of calcite cement.
12–13 ***Discoaster*** **spp.** displaying heavy overgrowth.
14 ***Reticulofenestra umbilicus*** lacking the central area delicate grid.
15 Distal shield of ***Ericsonia formosa*** partially fractured and dissolved. Dissolution also affects the elements of the distal central area.
16 Distal view of poorly preserved ***Coccolithus pelagicus*****.**
17 ***Isthmolithus recurvus*** fully coated by secondary calcite deposition.
18 Moderately preserved ***Discoaster saipanensis***.
19 ***Discoaster saipanensis*** to the left and ***Reticulofenestra umbilicus*** (>14 μm) to the right.

carbonate data (from Norris et al., 2014) and calcareous nannofossil biostratigraphy, which identify the most significant stratigraphic markers across the EOT.

3.1.2. ODP Site 1209

Calcareous nannofossils are generally common to abundant through the studied section. Strong dissolution (E2/E3) and very poor preservation (VP) characterize almost all the samples investigated in the lower part of the section (from ca. 145 to 141 adj. rmcd). The pervasive dissolution in the upper Eocene is also reflected in the high relative abundance (with respect to other taxa) of dissolution-resistant calcareous nannofossils and planktonic foraminifera, including *Globigerinatheka senni*, *Catapsydrax unicavus*, and *Globoturborotalita euapertura* (Bralower et al., 2002b). The preservation state improves slightly in the upper part, concomitant with an increase in overgrowth (Fig. 3). Calcareous nannofossil assemblages are characterized by extremely low diversity, high abundance of a few dominant dissolution-resistant taxa (e.g., *Discoaster*, *S. predistentus*, *Dictyococcites*), and by the sporadic occurrence of reworked taxa (e.g., *Chiasmolithus grandis*, *C. consuetus*, *C. solitus*, *Discoaster multiradiatus*). Reworking is more common (up to 8 specimens/mm^2) in the upper Eocene and in the uppermost part of the succession (up to 3 specimens/mm^2), where the assemblages show very poor preservation and strong etching. Despite all these issues, we obtained a reliable age model, based on the standard age-diagnostic taxa, which in this interval are mostly based on the presence of solution-resistant forms (Perch-Nielsen, 1979). The Top of *Hantkenina* spp. is, however, reported at 140.36 adj. rmcd (1209A-14H-5, 36–37 cm; Bralower et al., 2002a) well below the expected level when compared with both calcareous nannofossil biostratigraphy (Top of *D. saipanensis*) and isotope stratigraphy (LEE) (Fig. 3). The placement of the Top of *Hantkenina* spp. is often difficult, and stratigraphically depressed, due to its susceptibility to dissolution in the deep ocean and low abundances in neritic successions (Coxall and Pearson, 2007). For this reason, the Eocene/Oligocene boundary is very tentatively positioned at the Top of *Hantkenina* spp. but this is almost certainly too low with respect to the true extinction level. Linear sedimentation rates (LSRs) are extremely low for all the studied interval (mean value of 0.5 cm/kyr), especially during the upper Eocene and lower Oligocene. The succession spans nannofossil Zones CNE20 to CNO2 (Agnini et al., 2014) and has an estimated duration of 3.82 Myr.

3.1.3. Biostratigraphic data

Hole U1411B and Site 1209 provide a set of biohorizons that have been fundamental in constructing a biostratigraphic framework for the study sections and age models that allow for robust correlation between the two sites. These bioevents are either used in the biozonation of Agnini et al. (2014) or represent potentially useful patterns that require further testing. They are listed in stratigraphic order from older to younger (Figs. 2, 3; Table 1):

1. The Top of *C. reticulatum* marks the base of Zone CNE20 (Agnini et al., 2014) and occurs at 177.74 ± 0.31 mbsf at Hole U1411B, whereas at Site 1209 fragile specimens of *C. reticulatum* were not found, likely because of the pervasive dissolution observed in the upper Eocene samples.
2. At Hole U1411B, the Base of *S. predistentus* was found at 172.39 mbsf, within Chron C13r. At Site 1209, this species becomes abundant and continuous starting from 140.68 adj. rmcd. In the upper part of the Site 1209 section, we detected transitional morphologies that we grouped as *S. predistentus/S. distentus* morphotypes. *S. predistentus* is extremely abundant at Site 1209 (up to 284 n/mm^2), while at Hole U1411B the semi-quantitative abundance is lower (up to 19 n/mm^2).
3. The Top of *D. saipanensis* is used to define the base of Zone CNE21 and is usually found to occur ~300 kry after the Top of *D. barbadiensis* (Agnini et al., 2014). At Hole U1411B, the Top of *D. barbadiensis* (170.58 ± 1.44 mbsf) and the Top of *D. saipanensis* (167.87 ± 1.27 mbsf) are spaced and both lie within Chron C13r. At Site 1209, the synchronous extinction of *D. barbadiensis* and *D. saipanensis* at 139.73 adj. rmcd might indicate the presence of a short gap in sedimentation. Sporadic reworked specimens (1–4 n/mm^2) of these two species were documented through the succession above their Tops. In particular, the Top of *D. saipanensis* was located between the sample where the species is present and the sample where it is no longer present, while considering the rather complex distribution tail, the Top of *D. barbadiensis* was positioned between the range where the species distribution is continuous and the range where occurrence becomes discontinuous (Fig. 3).
4. The continuous presence and then marked increase in abundance of *C. subdistichus* gr. allows the base of Zone CNO1 to be identified (Agnini et al., 2014). At Hole U1411B, we identified the base of the major increase, here termed as Bi (Base of increase) of *C. subdistichus* gr., within Chron C13r at 154.71 ± 1.20 mbsf, 2.75 m above the extinction of *H. alabamensis* (Norris et al., 2014). A similar pattern for *C. subdistichus* gr., with comparable abundances, was documented at Site 1209, where this event was placed at a depth of 137.78 ± 0.22 adj. rmcd. The base of common and continuous (Bc) *C. subdistichus* gr. was found at a lower level in both the sections, at 172.39 ± 0.02 mbsf and 140.23 ± 0.13 adj. rmcd, respectively.
5. The Top of *E. formosa* defines the base of Zone CNO2 (Agnini et al., 2014). This biohorizon was placed at 130.80 mbsf at Hole U1411B, falling within Chron C13n. However, the position of the last occurrence of this taxon is not precisely located due to the low sampling resolution that leads to an error of ±2.8 m. At Site 1209, the Top of *E. formosa* occurs at 132.83 ± 0.08 adj. rmcd.
6. The Base of *S. akropodus* occurs at 133.85 ± 0.27 mbsf at Hole U1411B within Chron C13n, and at 134.20 ± 0.25 adj. rmcd at Site 1209.
7. The Top common of *C. subdistichus* gr. was reported at 117.02 mbsf (Hole U1411B) and at 130.98 adj. rmcd (Site 1209). These data are extremely consistent, falling 55% and 70% from the top of Zone CNO2, defined by the Top of *Reticulofenestra umbilicus*.
8. At Hole U1411B, *I. recurvus* is continuously present with relatively high abundances (up to 72 n/mm^2) and its Top common

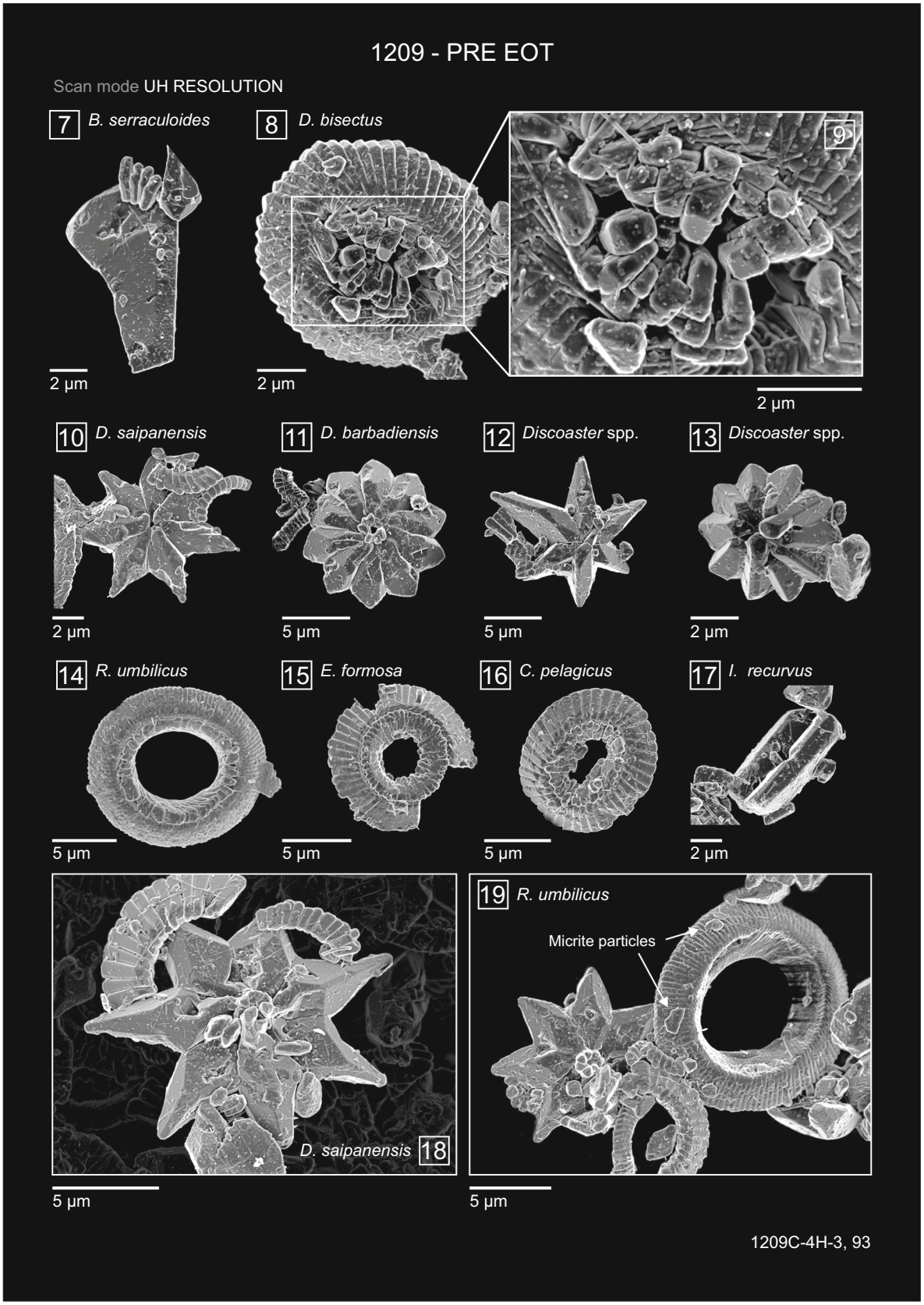

Fig. 7. (*continued*).

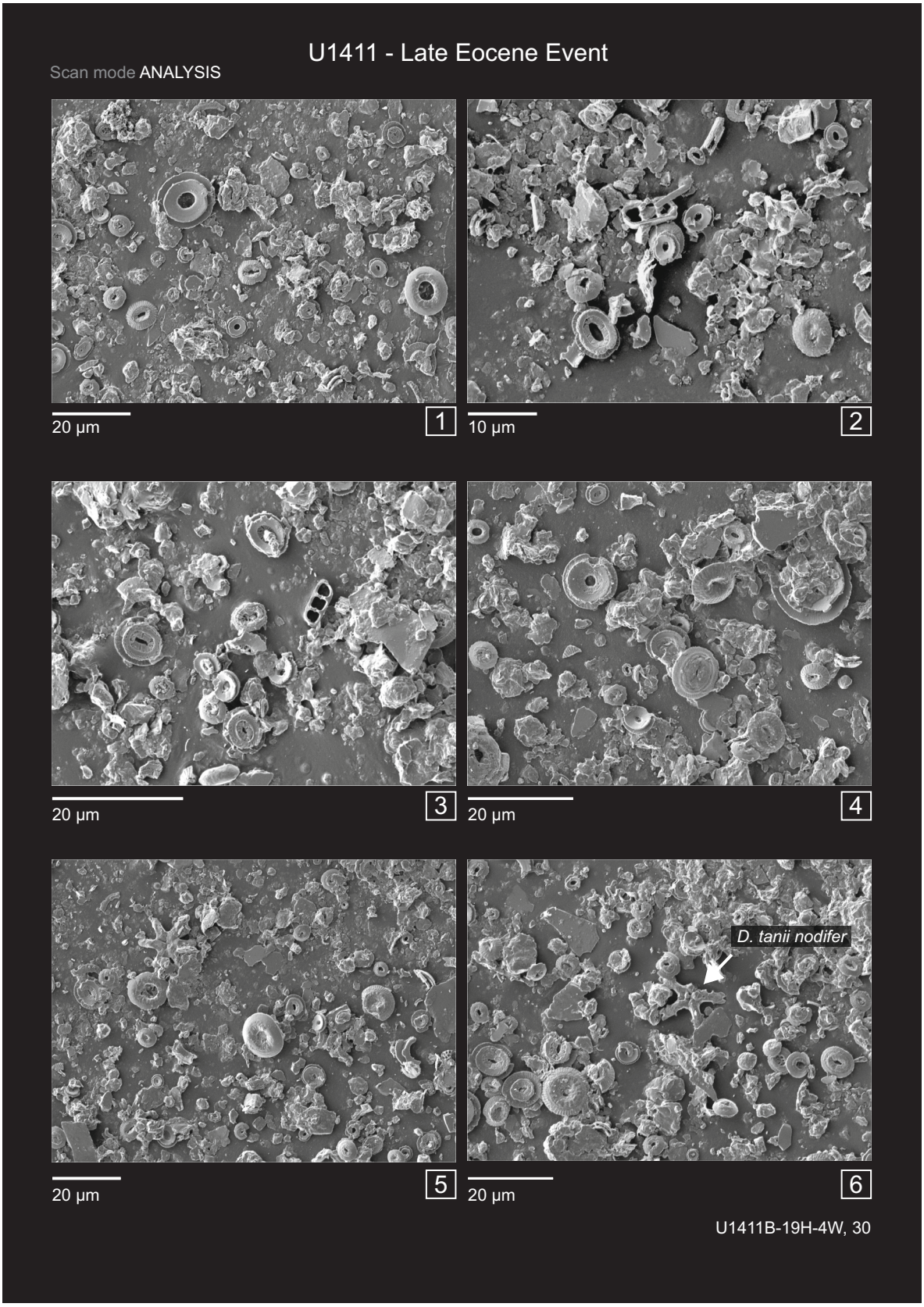

Fig. 8. Scanning electron photomicrographs showing the preservation of Late Eocene Event calcareous nannofossils from Site U1411 (sample U1411B-19H-4W, 30 cm). Insets:
1–6 Analysis scan mode micrographs showing the assemblage constituents.
7–8 Well preserved ***Reticulofenestra umbilicus*** (>14 µm) (7) with open central area spanned by delicate net remains (8).
9 Proximal view of ***Reticulofenestra daviesii*** with a robust grill with elongated perforations.

10 Distal view of ***Coccolithus pelagicus***.
11 ***Discoaster* cf. *D. tanii*** with a prominent stem on one side showing minor overgrowth.
12 ***Isthmolithus recurvus*** exceptionally well preserved.
13 ***Sphenolithus moriformis* gr.**, lateral view.
14 ***Dictyococcites bisectus*** shows no sign of dissolution and/or overgrowth.
15 Extremely well preserved specimen of ***Ericsonia formosa***.

(Tc) is detected at 130.80 ± 2.79 mbsf, coinciding with the Top of *E. formosa*. At Site 1209, the Tc of *I. recurvus* occurs at 133.33 ± 0.13 adj. rmcd, 0.50 m below the Top of *E. formosa,* within Zone CNO1. We also carefully studied the Top of *I. recurvus*, which occurs at 103.78 ± 1.58 mbsf (Hole U1411B) and at 128.05 ± 0.25 adj. rmcd (Site 1209).

9. The Top of *R. umbilicus* defines the base of Zone CNO3 (Agnini et al., 2014). At Site 1209 this was recorded at 126.68 adj. rmcd, whilst at Hole U1411B it occurs at 99.95 mbsf.
10. At Site 1209, we also identified abundant occurrences of *S. intercalaris* (up to 40 n/mm^2) in the upper Eocene.

3.2. Geochemistry (Site 1209)

At Site 1209, calcareous nannofossil biostratigraphy was correlated with a high-resolution (ca. 10 kyrs) bulk geochemical record (Fig. 4), which allows the subdivision of the studied section into different intervals based on distinctive trends and variations. The oxygen isotope values ($\delta^{18}O$) average 0.56 ± 0.38‰ (1σ), while the $\delta^{13}C$ data average 1.87 ± 0.30‰ (1σ) (Fig. 5). From the base of the section (142.40 adj. rmcd) to 140.90 adj. rmcd, we recognize relatively high positive $\delta^{18}O$ (up to 0.82‰) and $\delta^{13}C$ (up to 2.55‰) values. These values, recorded during the upper Eocene, coincide with an interval of extremely poor preservation, with high abundance peaks of discoasters (up to ~400 n/mm^2; Fig. 3). These data likely indicate a residual assemblage resulting from pervasive dissolution. Moreover, the low diversity of the assemblage and the absence of fragile taxa suggest that sediments were strongly affected by diagenetic processes in the lower part of the section. Based on these considerations, the anomalous $\delta^{18}O$ and $\delta^{13}C$ values from the lower part of the section will be discarded and any paleoenvironmental interpretations avoided (Fig. 4, dashed pink bar).

Stable isotopic values recorded above 140.90 adj. rmcd, however, are consistent with global deep-marine records with minimal alterations of original $\delta^{18}O$ bulk values, despite the presence of minor dissolution and major overgrowth observed throughout the succession. Between 140.90 adj. rmcd and 139.73 adj. rmcd, both $\delta^{18}O$ and $\delta^{13}C$ bulk values gradually start to increase. The interval between the bottom of the section and 139.73 adj. rmcd, corresponds to the "pre-EOT" phase. A transient positive $\delta^{18}O$ excursion from 0.32 to 0.67‰ (from 139.80 to 139.65 adj. rmcd) was recognized and interpreted as the Late Eocene Event (LEE; Hutchinson et al., 2021). The LEE transient event occurs very close to the extinction level of *D. saipanensis* (139.73 ± 0.13 adj. rmcd). Between 137.40 (33.89 Ma) and 136.45 adj. rmcd (33.67 Ma; T EOIS), $\delta^{18}O$ rapidly increases by 0.71‰, shifting from 0.20 to 0.91‰, which is interpreted as the EOIS and thus the end of the EOT. Above 136.45 adj. rmcd and up to 133.85 adj. rmcd, the oxygen isotopes record an interval of positive $\delta^{18}O$ values, with a maximum peak of 1.22‰ (135.20 adj. rmcd), corresponding to the EOGM (here termed the "EOGM" phase). From 133.85 adj. rmcd upsection, $\delta^{18}O$ values remain relatively stable with absolute relatively high values (0.82‰), a phase which is defined as "steady-state" in this work. The general trends in the carbon isotopes correlate with the main events recognized in the $\delta^{18}O$ curve, with no significant lags.

The bulk carbonate content (wt, %) of Site 1209 also shows high variability, with a mean value of 77.5%, whilst the carbonate content (wt, %) at Hole U1411B is considerably lower (14% - 55.21%; Norris et al., 2014).

3.3. Age models

The age models and correlation between the two sites are primarily based on calcareous nannofossil, oxygen stable isotope stratigraphy and magnetic reversal stratigraphy (Table 1). Using the same chronology, records at Hole U1411B and Site 1209 were aligned in the time domain.

The age model for Hole U1411B was constructed using calcareous nannofossil bioevents and magnetostratigraphic data (Norris et al., 2014) as tie-points (Table 1) based on the GTS20 (Gradstein et al., 2020), since oxygen stable isotope records were not available. Given the uncertainty of the Top of *E. formosa* (sampling error ±2.79 m), that is the result of low sampling resolution, we decided to exclude this datum from the age model. For ODP Site 1209, the age-depth model is constructed using nannofossil and oxygen stable isotope datums. At this site bio-chemostratigraphic constraints indicate a condensed sequence, characterized by very low sedimentation rate (average LSR of 0.5 cm/kyr). The synchronous tops of the two rosette-shaped discoasters (i.e., *D. barbadiensis* and *D. saipanensis;* 139.73 adj. rmcd) that are usually spaced in time (34.76 and 34.44 Ma; GTS20 - Gradstein et al., 2020) supports the presence of a short hiatus especially considering the high sampling resolution (ca. 10 kyr).

3.4. Preservation of calcareous nannofossils

Samples from Hole U1411B and Site 1209 have been visually compared with the help of SEM analyses to evaluate the state of preservation of the calcareous nannofossils. We selected four samples from Hole U1411B collected from four different time slices across the late Eocene – early Oligocene: the first sample from the "pre-EOT" phase (below the Top of *D. saipanensis*; 34.44 Ma), the second sample from the Late Eocene Event - LEE (corresponding to the Top of *D. saipanensis*), the third sample from within the EOT (bracketed by the two positive Step 1 and EOIS $\delta^{18}O$ excursions and corresponding to most of Chron C13r) and the fourth sample from the EOGM (starting from the top of the EOIS including the highest $\delta^{18}O$ values). An equal number of comparative samples were selected from ODP Site 1209 from the same phases. The position of these samples is shown in Fig. 2 and Fig. 3 along with the carbonate record. A brief description of the calcareous nannofossil assemblage compositions and preservation is provided below, summarizing the main SEM observations.

3.4.1. Pre-EOT phase

IODP Site U1411 (Sample U1411B-21X-CC, 25–33 cm). The upper Eocene calcareous nannofossil abundances range from few to common, with moderate to good preservation and no sign of dissolution or recrystallization. The carbonate content is relatively low as reported in Fig. 2 and shipboard data (20–30%; Norris et al., 2014). The sample is dominated by clay minerals that may derive from detrital sources or from authigenic or late-stage mineral growth. In our investigation clay seems to occur as small plates (Fig. 6; inset 4). The clay-rich ooze contains well-preserved coccoliths, as shown by the intact specimens of *Coccolithus*, *Clausicoccus*, *Ericsonia*, *Cribrocentrum*, and *Reticulofenestra* (Fig. 6; insets 16, 17, 23, 18, and 24). The latter two still retain the fine nets of the central area. Late Eocene nannoliths (rosette-shaped

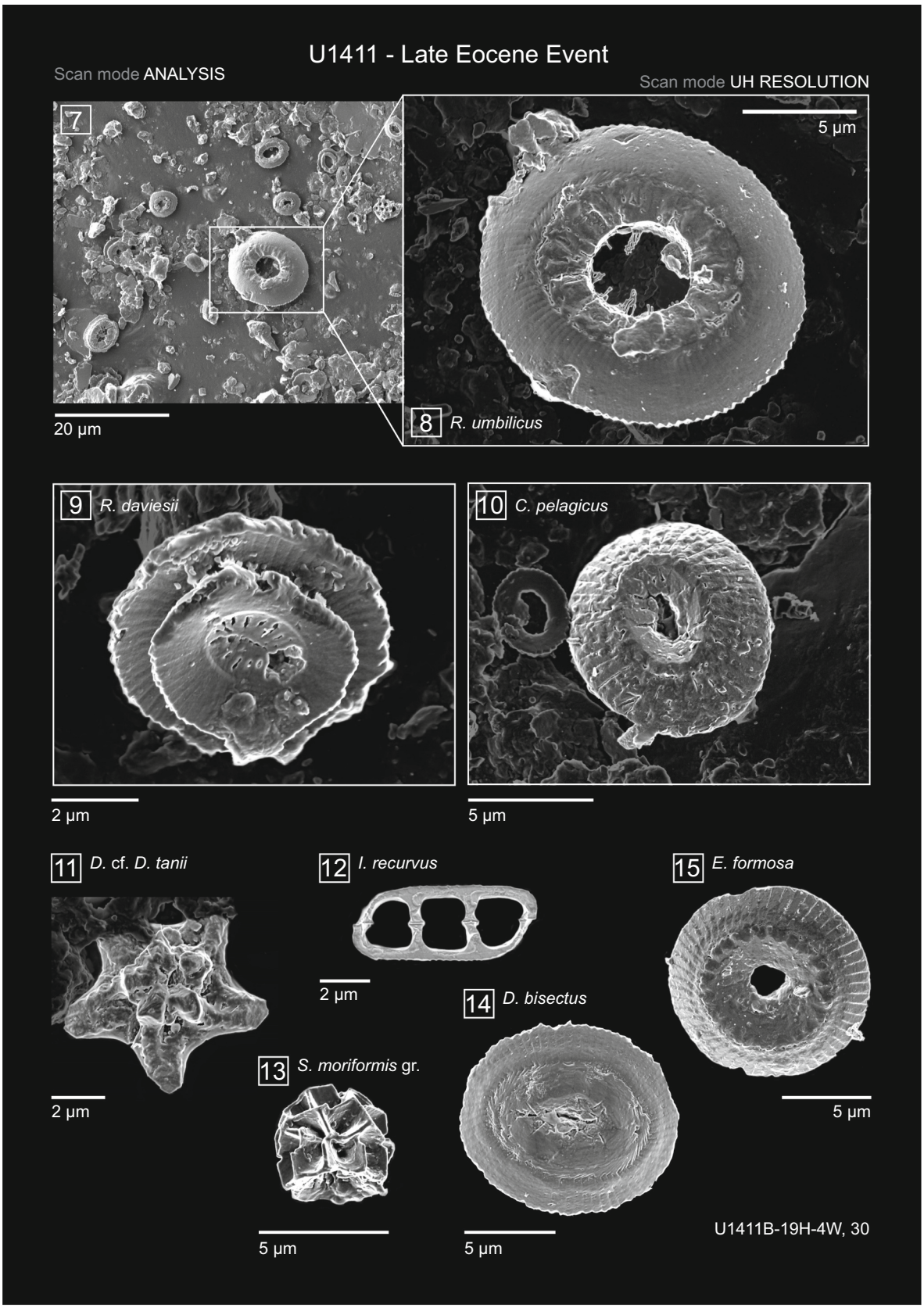

Fig. 8. (*continued*).

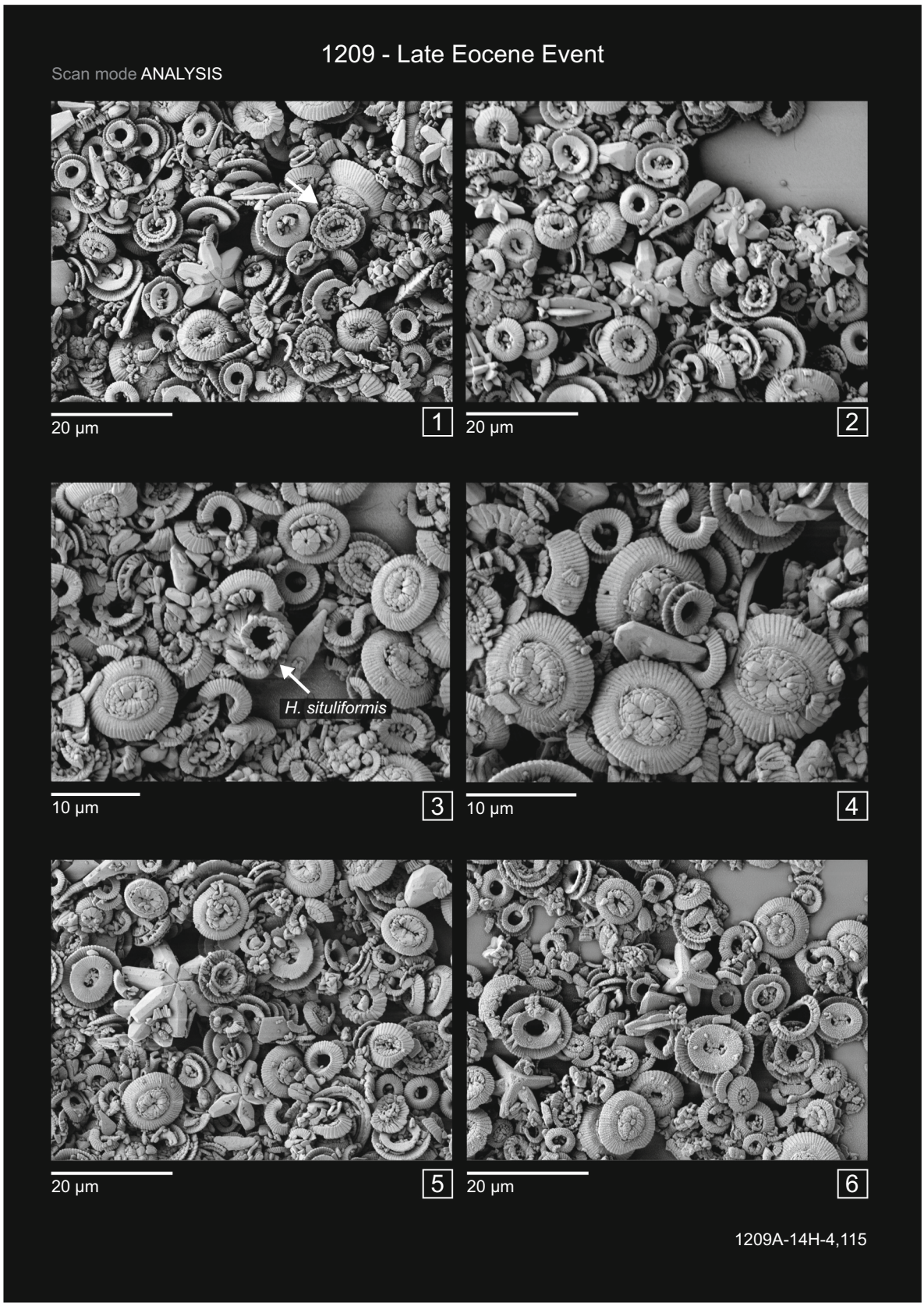

Fig. 9. Scanning electron photomicrographs showing the preservation of Late Eocene Event calcareous nannofossils from Site 1209 (sample 1209A-14H-4W, 115 cm). Insets:
1–6 Analysis scan mode micrographs showing the assemblage components. The arrow (1) shows the welded elements of the proximal shield that characterize most of the placoliths.
7 ***Discoaster tanii*** showing euhedral crystal faces along the rays.

8 Distal view of ***Dictyococcites bisectus*** showing extreme overgrowth of its central plug. Some fragments and other taxa are cemented to its shield.
9 Broken wall of a **calcisphere** showing the mosaic grains.
10 Unknown placolith (probable small *Calcidiscus* sp.).
11 ***Ericsonia formosa*** showing an extremely well-preserved external rim that gives to the placolith a smooth circular outline. The elements of the central area are characterized by severe recrystallization.
12 ***Reticulofenestra umbilicus*** in distal view lacking the central area net.
13 Protococcolith ring of ***Dictyococcites* spp.**
14 ***Sphenolithus pseudoradians*.**
15 Several specimens of ***Dictyococcites bisectus*** showing differential growth of the central plug elements by accretion of secondary calcite.
16 Micrographs showing some of the major assemblage constituents, including ***Sphenolithus moriformis, Dictyococcites* spp.*, Reticulofenestra* spp.**. An "euhedral" ***Discoaster* spp.** is also shown, the center of which is pitted (as reported by the arrow).

discoasterids) dominate the assemblage, showing no signs of secondary overgrowth. The most common species are *D. barbadiensis* and *D. saipanensis*.

We also documented the presence of *Discoaster robustus*, whose stem is barely distinguishable from the body, and forms a pyramid-like structure (Fig. 6; insets 13–15). Many well-preserved specimens of *C. reticulatum*, with their delicate grid in the central area, were observed in the sample (Fig. 6; inset 18).

ODP Site 1209 (Sample 1209C-4H-3, 93 cm). The pre-EOT interval at Site 1209 coincides with a phase of strong dissolution and reworking. Reworked taxa are mainly from the middle-upper Eocene and include *C. grandis*, *C. consuetus*, *C. solitus*, *D. multiradiatus*, and *S. spiniger*. The carbonate content of the sample is ca. 80%. Placoliths of *E. formosa* are extremely affected by dissolution (Fig. 7; inset 15) and the most common components of the assemblage are represented by fragments of coccoliths where the proximal and distal shield are usually separated. These broken coccoliths belongs to relatively large *Dictyococcites* and *Reticulofenestra,* which are known to be extremely resistant to dissolution.

The presence of isolated coccolith shields, widened central areas and micrite particles generally characterize strongly etched samples (Hill, 1975). Poorly preserved distal shields of *C. pelagicus* occur together with well-preserved ones. Dissolution processes seems to primarily affect distal shields, especially corroding the central area of *E. formosa*, as reported by preliminary LM observations and counts, where several specimens of *E. formosa* were strongly affected by dissolution (Fig. 3). Fragmentation and dissolution are accompanied by severe overgrowth of discoasters and other solution-resistant forms. In some cases, discoasters are indeterminable due to secondary calcite deposition, especially along their rays. The calcite accretion is particularly evident in some specimens (Fig. 7; insets 12, 13), which show differential growth of their elements (rays or stem).

The original structure of *B. serraculoides* and *I. recurvus* is also masked by thick secondary calcite overgrowth (Fig. 7; insets 7, 17). The preferential deposition of calcite overgrowth strongly depends on the taxon considered: in the case of *D. bisectus* considerable amounts of calcite are deposited in the central plug (Fig. 7; insets 8, 9). Many specimens of *R. umbilicus* have lost their grid in the central area (Fig. 7; insets 14, 19). Small and fragile specimens are extremely rare to absent. All these observations confirm the hypothesis that the assemblage has been substantially altered by diagenetic processes.

3.4.2. Late Eocene Event

The Late Eocene Event (LEE) represents a crucial point of the Eocene-Oligocene transition, so far relatively understudied. This event includes an important change in the phytoplanktonic assemblage: the extinction of the last member of the rosette-shaped discoasters (i.e., *D. saipanensis*). After this, discoaster assemblages include only stellate, free-rayed morphotype which can be ascribed to several different species including *D. tanii* gr., *D. distinctus* and *D. deflandrei*.

IODP Site U1411 (Sample U1411B-19H-4W, 30 cm). Preservation is similar to the previous sample (U1411B-21X-CC, 25–33 cm), with calcium carbonate content remaining low (Fig. 2). The rosette-shaped discoasters are replaced by stellate discoasters. Specimens of *Discoaster* show varying degrees of preservation state within the same sample: some are well preserved with prominent lateral nodes on their rays and ray-end bifurcations (Fig. 8; inset 6), while others show a degrees of overgrowth (Fig. 8; inset 11). The good preservation of this sample is also confirmed by the presence of extremely well-preserved specimens of *R. umbilicus*, *R. daviesii* and *I. recurvus* (Fig. 8; insets 7–9, 12) and by the dissolution-resistant species *D. bisectus*, which shows no signs of overgrowth (Fig. 8; inset 14).

ODP Site 1209 (Sample 1209A-14H-4W, 115 cm). By contrast to the previous sample (U1209C-4H-3W, 93 cm), which exhibited fragmentation, dissolution, and overgrowth, this sample is almost exclusively dominated by recrystallization. Calcareous nannofossils show strong signs of secondary calcite reprecipitation, that has resulted in the formation of massive, overgrown forms, including *Dictyococcites*, *Discoaster* and *S. pseudoradians.* Fragmented coccoliths are very common and constitute the groundmass of the sediment. Accretion of secondary calcite is evident along the *Discoaster* arms, with the development of distinct (euhedral) crystal faces (Fig. 9; inset 7). This sample is characterized by the presence of common calcispheres (Fig. 9; inset 9) and specimens of *Hayella situliformis* (Fig. 9; inset 3). The dominant component of the assemblage is *Dictyococcites*, which is almost completely overgrown by accretion of calcite on the central plug (Fig. 9; insets 4, 15). An interesting note is that *E. formosa* exhibits the preferential deposition of overgrowth on the elements surrounding the central area (Fig. 9; inset 11).

3.4.3. Eocene-Oligocene Transition (EOT)

IODP Site U1411 (Sample U1411B-17H-7A, 25 cm). The high clay content of this sample has resulted in an extremely well-preserved assemblage, dominated by abundant and exceptionally preserved specimens of *C. subdistichus* gr. (Fig. 10; insets 7, 8, 13). *I. recurvus* is a taxon that is extremely susceptible to secondary overgrowth but the excellent preservation here is indicated by ribs conserved on the lateral side and transverse segments (Fig. 10; insets 11, 12). These ultrastructural details are obliterated at Site 1209. The exceptional preservation is also confirmed by the presence of complete coccospheres, which are typically encountered in clay-rich hemipelagic sediments (Bown et al., 2014), for example the occurrence of a coccosphere ascribed to *E. formosa* (Fig. 10; insets 17, 18). Reticulofenestrids (e.g., *R. umbilicus* and *R. daviesii*) retain their pristine and fragile central nets (Fig. 10; insets 16, 19) and the original structure is preserved in the small base of *B. serraculoides* (Fig. 10; inset 14).

ODP Site 1209 (Sample 1209C-3H-6, 90 cm). The sample is characterized by common to abundant nannofossils, which are partially dissolved – especially along the edges of the distal shields and in the central area – and then heavily recrystallized. In this carbonate-rich (~83%) ooze, *S. predistentus* is common and its bifurcated spines are commonly observed as broken fragments (Fig. 11; inset 1), usually overgrown (Fig. 11; insets 7, 8). Fragments of foraminiferal tests and

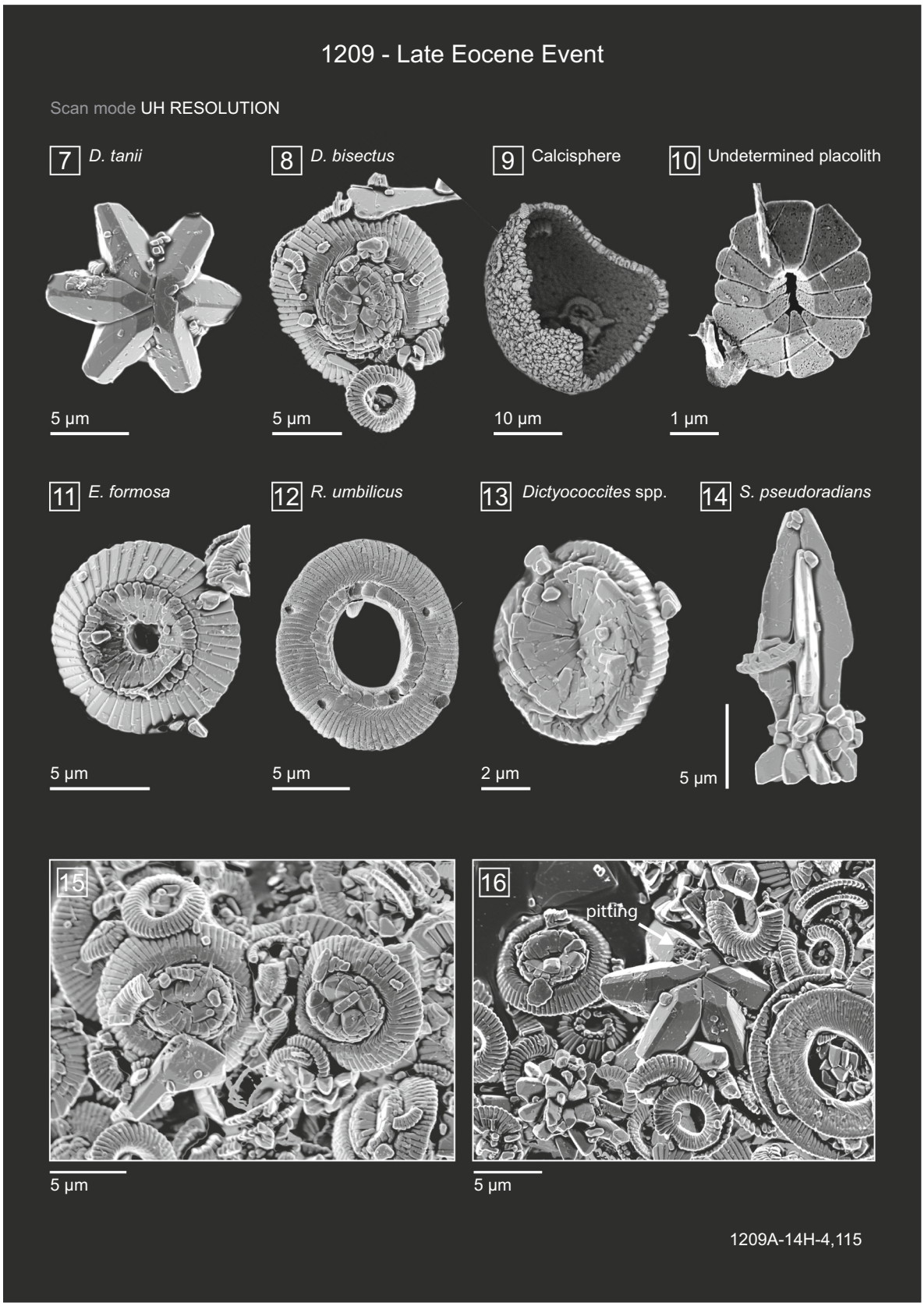

Fig. 9. (*continued*).

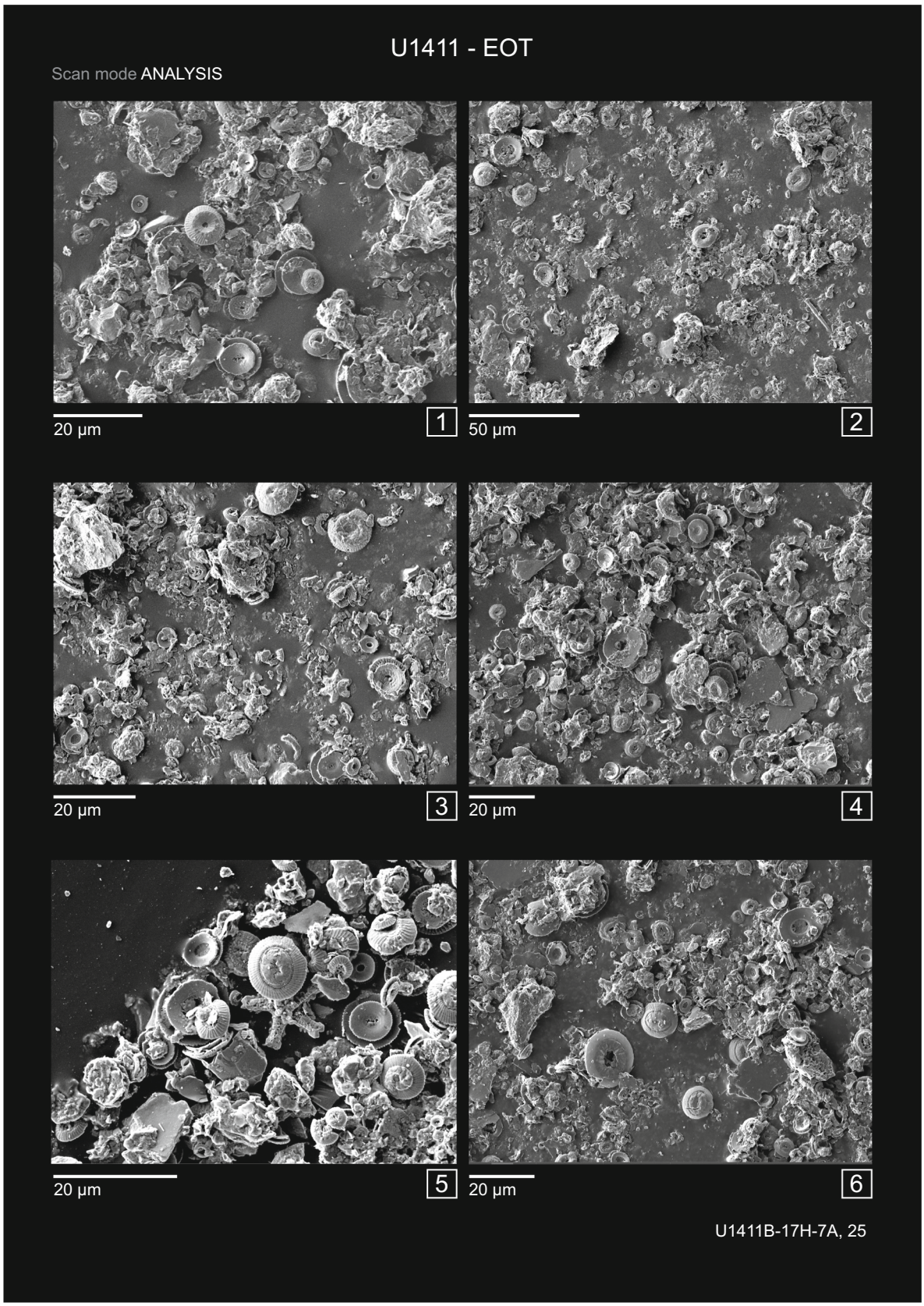

Fig. 10. Scanning electron photomicrographs showing the preservation of EOT calcareous nannofossils from Site U1411 (sample U1411B-17H-7A, 25 cm). Insets:
1–6 Analysis scan mode micrographs showing the assemblage constituents.
7–8 ***Clausicoccus subdistichus*** distal view.
9 ***Ericsonia formosa*** distal view.
10 ***Pontosphaera* spp.**.

11–12 ***Isthmolithus recurvus*** specimens showing exceptional preservation.
13 ***Clausicoccus subdistichus*** proximal view.
14 Proximal view of the basal disc of ***Bramletteius serraculoides***, which is slightly dissolved along the edges.
15 ***Isthmolithus recurvus*** overlaying a placolith.
16 Proximal view of ***Reticulofenestra umbilicus*** displaying the central grid.
17–18 Coccosphere of ***Ericsonia formosa*** acquired with the analysis scan mode (17) and with UH resolution scan mode (18).
19 Proximal view of ***Reticulofenestra daviesii***.
20 ***Sphenolithus moriformis***.
21 ***Discoaster tanii nodifer***.
22 ***Coccolithus pelagicus***.

calcispheres are also common (Fig. 11; insets 3, 6). *H. situliformis* is abundant in this sample. *Discoaster* and *Dictyococcites* accreted a large amount of secondary calcite forming a thick overgrowth along the rays and in the central plug, respectively (Fig. 11; insets 9, 10, 12). Sporadic specimens of *Chiasmolithus* without the central cross were found during the LM investigation. Also in this sample, the central holes of *I. recurvus* are infilled by calcite overgrowth.

3.4.4. Earliest Oligocene Glacial Maximum (EOGM)

IODP Site U1411 (Sample U1411-16H-1W, 50 cm). Calcareous nannofossils from the EOGM at IODP Site U1411 are extremely well-preserved. However, some morphological features are slightly obscured by a thin film of clay that persists despite the intensive treatment carried out to remove it (Fig. 12; insets 1–6). The sample is characterized by several specimens of *I. recurvus* (Fig. 12; inset 8), *Blackites* (Fig. 12; inset 10), rhabdolith fragments (Fig. 12; inset 16), small reticulofenestrids (e.g., *R. minuta*), *Pontosphaera* (Fig. 12; insets 7, 18) and *Helicosphaera* (Fig. 12; inset 21). The optimal preservation permits the observation of a finely perforate grill on the proximal side of *C. subdistichus*. These micro-pores are visible underneath the larger ones in the distal shield (Fig. 12; inset 11, 13).

ODP Site 1209 (U1209-3H-5, 35 cm). The sample is characterized by very high carbonate content (82%) with recrystallization being the dominant diagenetic factor. Many fragments of planktonic foraminifera (Fig. 13; inset 1) are present. Several placoliths, often difficult or impossible to identify, have proximal shields elements welded together by secondary calcite accretion (Fig. 13; inset 16). The sample is characterized by extreme abundances of heavily-resistant calcareous nannofossils, including many placoliths of *Dictyococcites* (Fig. 13; insets 9, 19), *Reticulofenestra* (Fig. 13; inset 11), *Coccolithus* (Fig. 13; inset 12), *B. serraculoides* (Fig. 13; insets 17, 18) and *Sphenolithus* (Fig. 13; inset 10).

4. Discussion

4.1. Biostratigraphic frameworks

We have compared the biostratigraphic events and quantitative distribution patterns (Fig. 2 and Fig. 3) seen at Hole U1411B and Site 1209, from section base to top:

- The Top of *C. reticulatum* was identified at Hole U1411B, but not found at Site 1209. The absence of *C. reticulatum* may be explained by ecological factors but is more likely a preservation artifact resulting from the extremely poor preservation at the base of the Site 1209 study section. This hypothesis is consistent with the fact that this species is thought to be relatively prone to dissolution (Toffanin et al., 2013).
- The reliability of the Base of *S. predistentus* is much debated, because of the scattered presence of this sphenolith close to its first appearance. We found that the base of this event slightly predates the extinction of rosette-shaped discoasters at both the studied sites, lying in the upper part of Zone CNE20, as also reported by Fioroni et al. (2015). However, the position observed at Site 1209 and Hole U1411B is not consistent with that recorded at Site 756, where the Base of this species was found later within CNO2 (Viganò et al., 2023). Therefore, we propose that this event may be diachronous or, at the very least, differs between the two studied oceans, namely the Pacific and the Indian oceans.

  Differences in abundances between Site 1209 (0–284 n/mm^2) and Hole U1411B (0–19 n/mm^2) are likely related to both preservation and ecological preferences, since Site 1209 has been interpreted as being characterized by probable warm and oligotrophic conditions while Site U1411 was located in a more eutrophic environment (Schneider et al., 2011; Cappelli et al., 2019).
- The identification of the Base common of *C. subdistichus* gr. presents challenges (Viganò et al., 2023) because determining the precise start of the acme interval is objectively difficult. At different sites, this taxon shows different relative and absolute abundances, and it is thus impossible to define its Base of common and continuous abundance with a single threshold value, applicable across sites. This issue results in a certain degree of uncertainty, though the acme interval itself surely represent a valuable tool to correlate earliest Oligocene successions.
- The Top common of *I. recurvus* is inconsistently reported, suggesting that this bioevent should be applied with caution. In particular, the ranking between the Tc of *I. recurvus* and the Top of *E. formosa* seems to be problematic. For example, at Site 1209, the Tc of *I. recurvus* was recorded at 33.01 Ma. Conversely, the Top of *I. recurvus* is well recognized at Site 1209 and Hole U1411B, with an age of 32.19 and 32.14, respectively. However, its extinction is commonly considered "one of the most inconsistent datums" (Berggren et al., 1995).
- The Base of *S. akropodus* documented at Site 1209 and Hole U1411B (age estimate of 33.19 Ma and 33.38 Ma, respectively) is consistent with records from the South Atlantic (Site 1263; Bordiga et al., 2015), being found in the upper part of Zone CNO1. The age estimate reported from the Indian Ocean (Site 756) of 33.26 Ma (Viganò et al., 2023), is also consistent. It has also been reported at a similar level from the northeastern Atlantic Ocean (de Kaenel and Villa (1996), where it was used to approximate the Zone NP21/NP22 boundary. Nonetheless, our result is in disagreement with that reported by Fioroni et al. (2015) who extended this species down to the upper Eocene, within Chron C13r. Apart from this minor discrepancy, available data seem to confirm that the base of *S. akropodus* could represent a valid and reliable marker, helping to further subdivide the long duration Zone CNO1.
- The Top common of *C. subdistichus* gr., reported at Hole U1411B (age estimate of 32.71 Ma) and at Site 1209 (age estimate of 32.62 Ma), seems to be fairly consistent and reliable, as previously suggested (Viganò et al., 2023), being constantly found above the Top of *E. formosa*, within Chron C12r.
- The Top of *R. umbilicus* is not easy to detect because of the scattered occurrences of the taxon in the final 'tail' of its distribution.

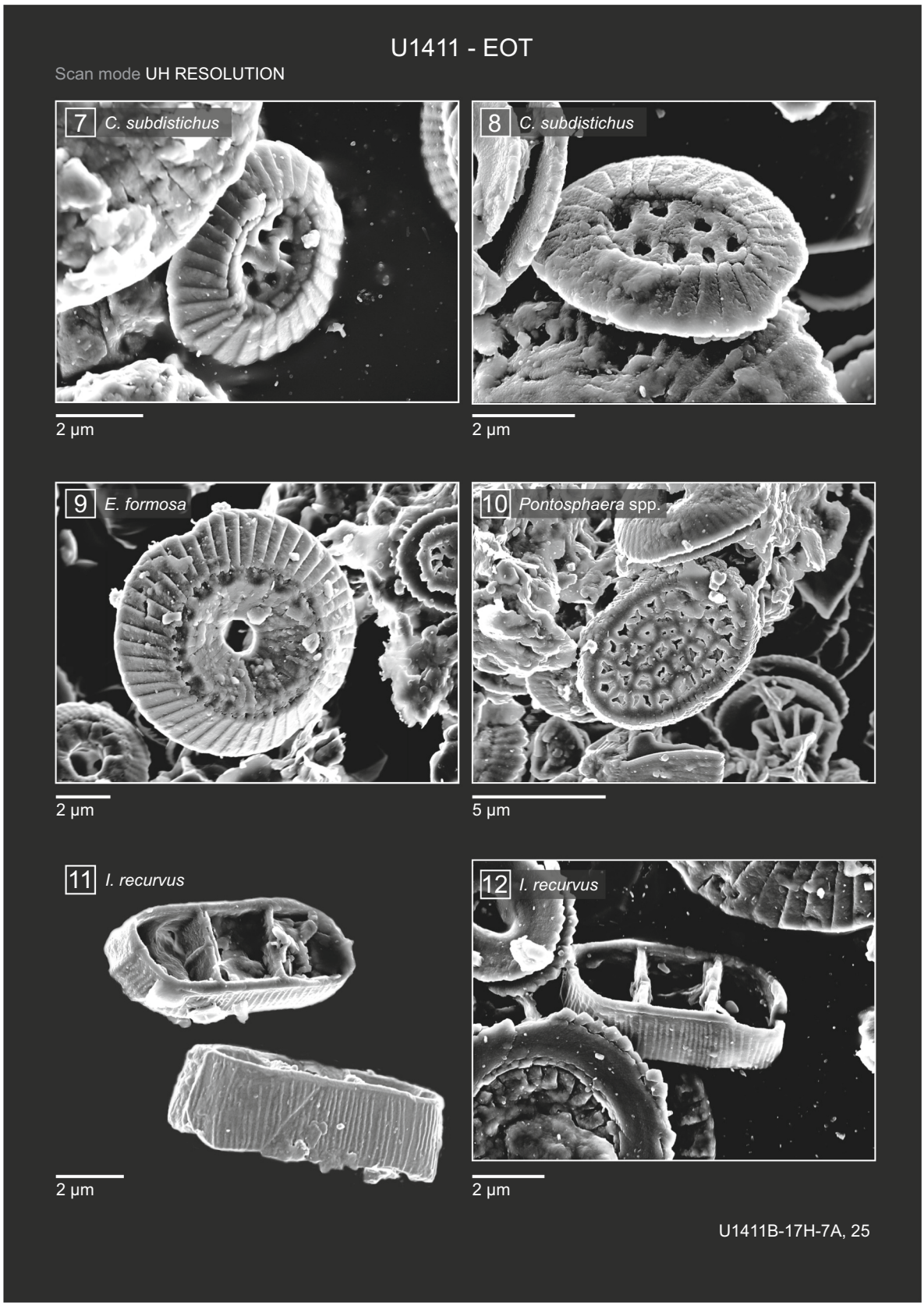

Fig. 10. (*continued*).

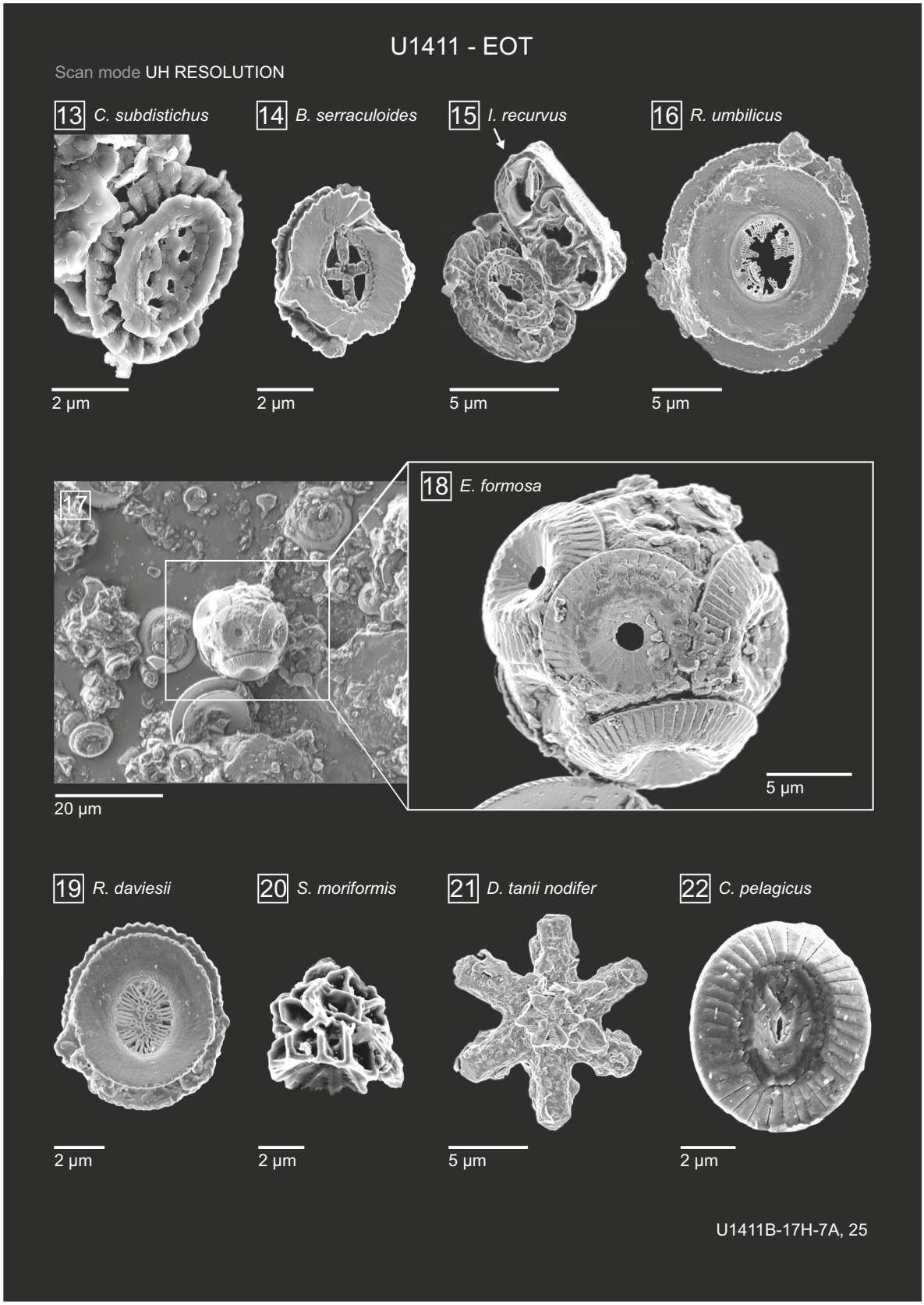

Fig. 10. (*continued*).

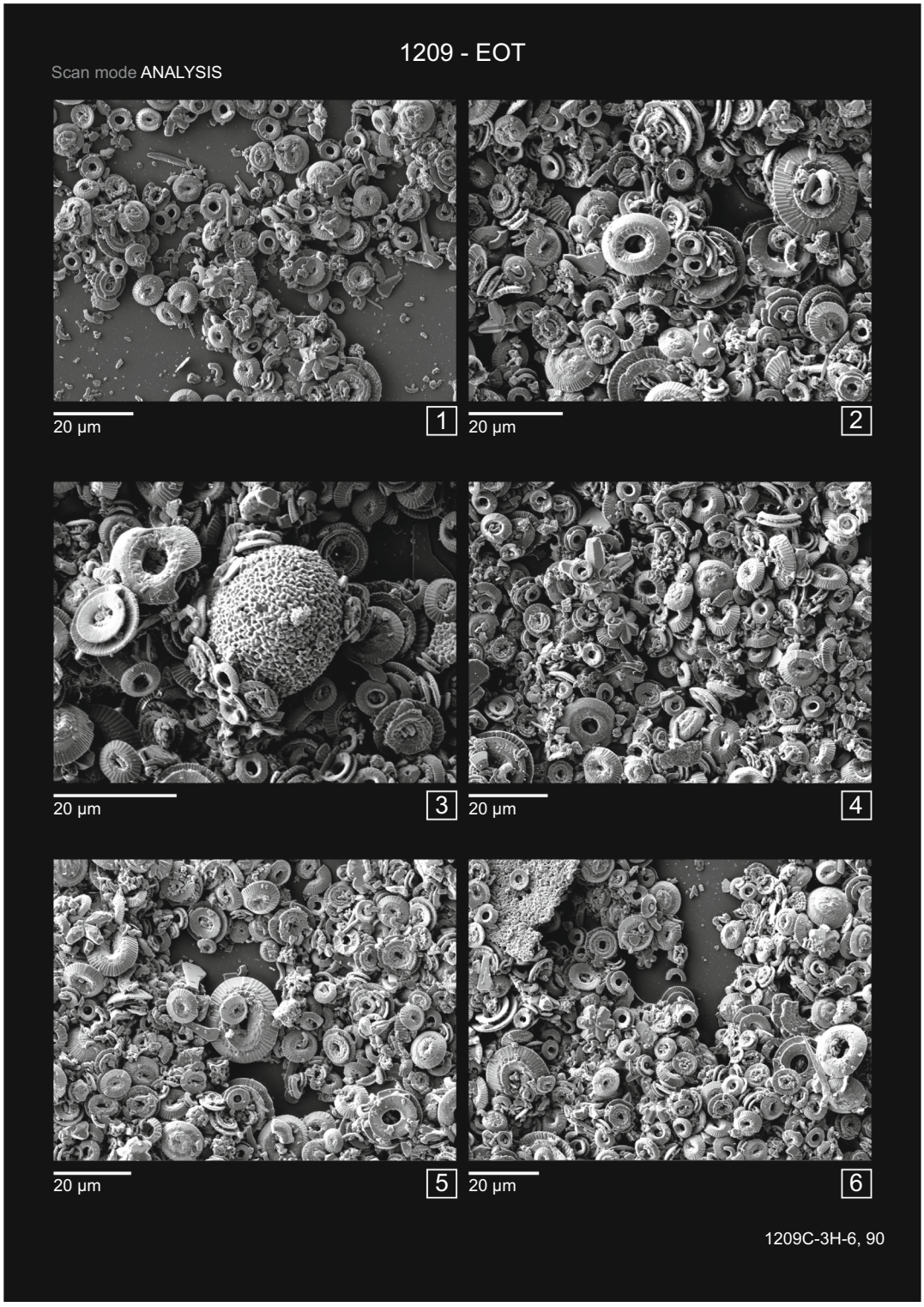

Fig. 11. Scanning electron photomicrographs showing the preservation of EOT calcareous nannofossils from Site 1209 (sample 1209C-3H-6, 90 cm). Insets:
1–6 Analysis scan mode micrographs showing the assemblage constituents.
7–8 ***Sphenolithus predistentus*** acquired with the analysis scan mode (**7**) and with UH resolution scan mode (8).
9–10 ***Discoaster*** **spp.** in UH resolution (9) and analysis scan mode (10). The specimen shows heavy overgrowth.

11 ***Coccolithus pelagicus*** with the R elements of the upper tube slightly overgrown.
12 ***Dictyococcites bisectus*** with secondary calcite overgrowths in the central plug.

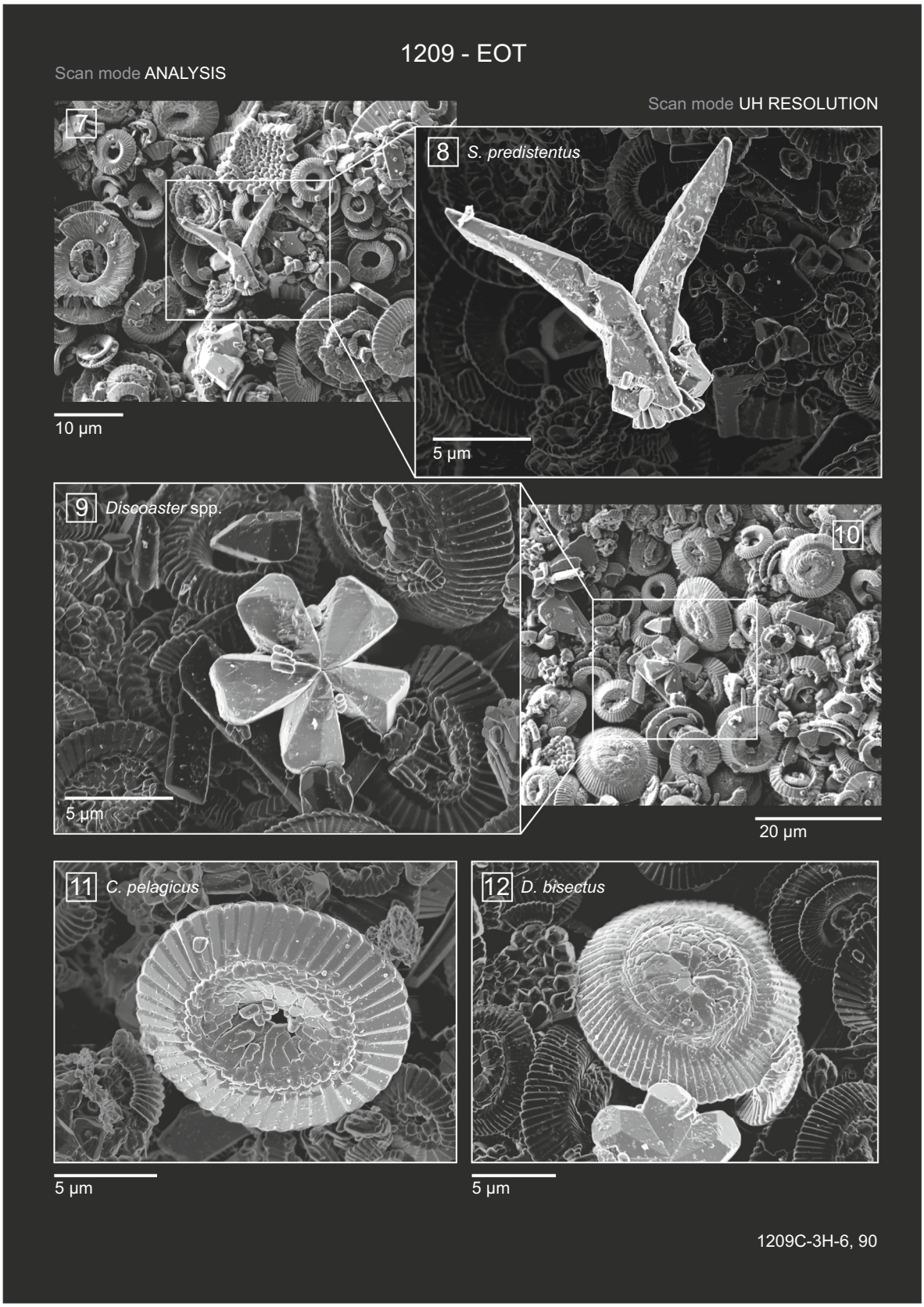

Fig. 11. (*continued*).

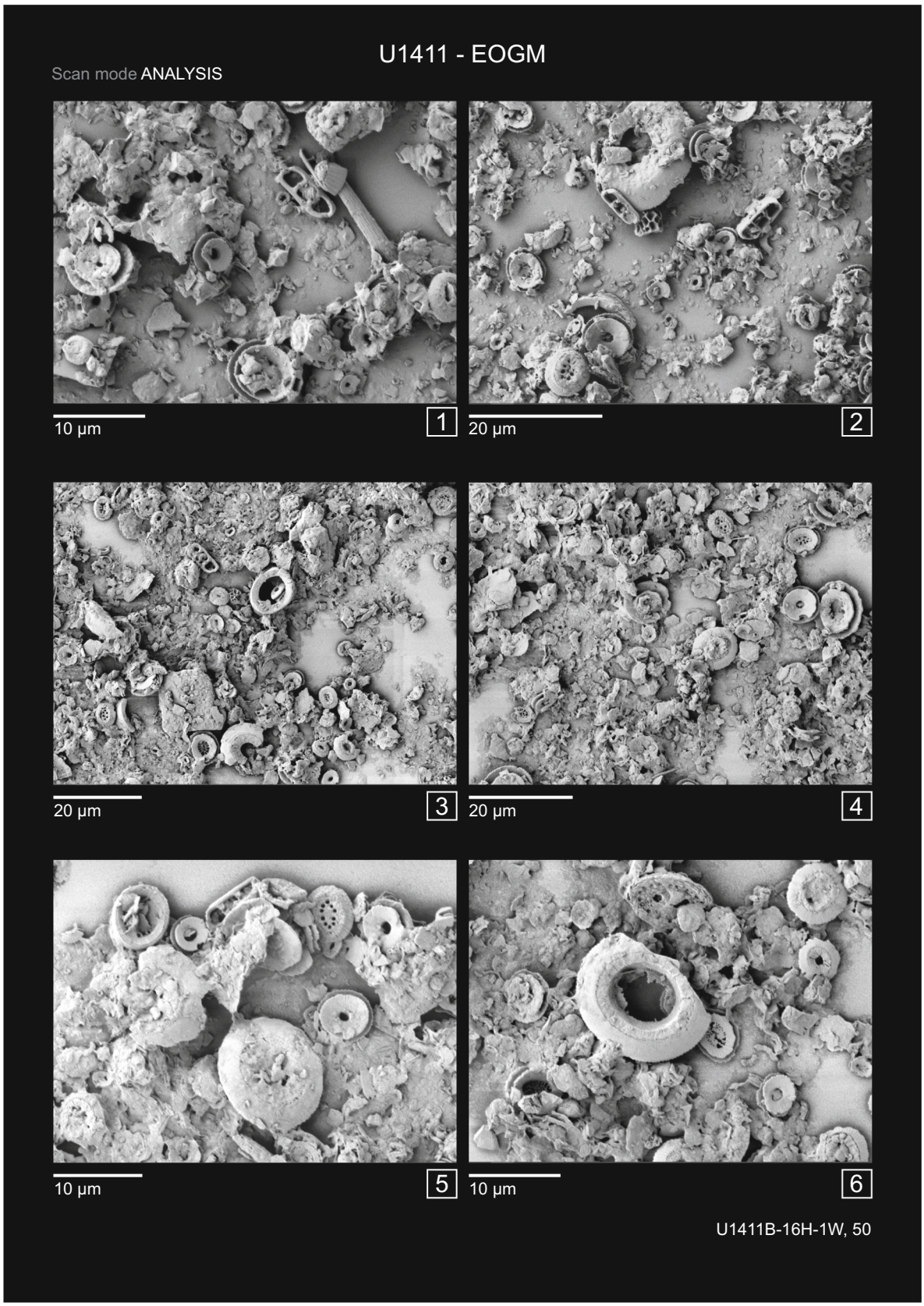

Fig. 12. Scanning electron photomicrographs showing the preservation of EOGM calcareous nannofossils from Site U1411 (Sample U1411-16H-1W, 50 cm). Insets:
1–6 Analysis scan mode micrographs showing the assemblage constituents, which are partly covered by a thin coating of clay minerals.
7 ***Pontosphaera*** **spp.**.
8 ***Isthmolithus recurvus***.
9 ***Dictyococcites bisectus*** showing exceptional preservation.

10 ***Blackites*** **spp.**
11 ***Clausicoccus subdistichus*** (distal side) with visible micro-pores, and a small reticulofenestrid (proximal side).
12 ***Ericsonia formosa*** distal shield.
13 ***Reticulofenestra umbilicus*** with ***Clausicoccus subdistichus*** leaning over.
14 ***Discoaster distinctus.***
15 Proximal side of ***Reticulofenestra umbilicus.***
16 ***Sphenolithus moriformis*** and a spine fragment of ***Blackites*** **spp.**.
17 Proximal view of ***Reticulofenestra dictyoda.***
18 ***Pontosphaera pulcheroides.***
19 Undetermined coccosphere.
20 ***Bramletteius serraculoides*** base.
21 ***Helicosphaera reticulata.***

At Site 1209, the occurrence of *S. intercalaris* in the upper Eocene (up to 40 n/mm^2) is consistent with previous studies from Shatsky Rise (Site 1208; Bown, 2005), Equatorial Pacific (Toffanin et al., 2013) and Tasman Sea (Viganò et al., in prep.; up to 22 n/mm^2). Therefore, the presence of this taxon is well documented in the Pacific Ocean. However, no evidence of the presence of *S. intercalaris* was reported from the North Atlantic (Hole U1411B; this study) or from the Indian Ocean (Hole 756C; Viganò et al., 2023).

4.2. Reconstructing past preservation

Since the 1970's, the availability of the scanning electron microscope (SEM) and the beginning of the study of the deep-sea cores promoted an explosion in the study of diagenetic processes on calcareous nannofossil assemblages (van der Lingen and Packham, 1975). The landmark works by Fisher et al. (1967) and Adelseck et al. (1973) provided general trends as diagenesis becomes more pervasive: small coccoliths tends to disarticulate along sutures due to dissolution, producing large amounts of micron-sized particles; placoliths with overlapping elements in the distal shields offers greater resistance to dissolution; discoasters tend to overgrow with the precipitation of highly euhedral calcite, becoming several times more massive than the original; larger coccoliths tend to persist in highly recrystallized sediments. Accordingly, recrystallization and dissolution severely affect nannofossils, and may result in the loss of the pristine ecological and geochemical signal. Understanding how preservation affects the phytoplankton thanatocenosis can help in disentangling paleoenvironmental information from diagenetic overprint. Our qualitative SEM study provides a detailed picture of the variations that occur in the nannofossil assemblages throughout the studied interval. Furthermore, the comparative LM and SEM observations have been useful in understanding how diagenetic alteration can modify the assemblage. Once you have found a way to evaluate how the different components of the sediment are altered what remains to understand is to determine where these changes have occurred. Although there are no conclusive elements to support a single hypothesis, it seems plausible to hypothesize that the diagenetic processes that have extensively altered the nannofossil assemblages occurred either at the water-sediment interface or just below it, especially considering the low sediment accumulation rates (or even the presence of depositional gaps) that led to prolonged exposure of fossil remains on the ocean floor or in its immediate vicinity (Bathurst, 1972; Burdige, 2007; Morse, 2003). The pore waters may have acted as agents of dissolution and subsequent recrystallization, emphasizing the diagenetic modifications that occurred early when the sediments were exposed on the sea floor. Previous results from EOT sediments (e.g., Dunkley Jones et al., 2008; Bordiga et al., 2015; Jones et al., 2019) suggest a quite homogeneous response of calcareous nannofossils to the environmental changes that occurred during the E-O transition. A possible interpretation is that productivity and temperatures changed globally in the same direction and thus quite similar paleoenvironmental changes are recorded in sediments where coccoliths are characterized by comparable states of preservation. However, in diagenetically affected sediments, as is the case of Site 1209, paleoecological interpretations should be avoided or approached with extreme caution because the fossil nannoplankton assemblages are deeply biased by taxon-dependent preferential dissolution. At ODP Site 1209, our morphological analysis suggests that diagenetic processes have significantly influenced the morphological variations and the presence and/or relative abundances of certain taxa. These diagenetic alterations have played a crucial role in shaping the observed patterns.

In particular, the morphological variations detected in the studied samples mainly consist of the dissolution of more delicate structures, such as nets (e.g., in reticulofenestrids), holes (e.g., in *Clausicoccus*), or the circular opening of *E. formosa*. Additionally, other variations included the overgrowth of certain elements, such as the ribs of *I. recurvus*, the base and apical spine of *S. predistentus*, the rays of discoasters, and the solid central plug of *D. bisectus*.

In the critical pre-EOT phase at ODP Site 1209, the assemblage is the result of strong dissolution (E3). Despite this, the most resistant and biostratigraphically/ecologically diagnostic forms (i.e., rosette-shaped discoasters and *E. formosa*) are still present, even though altered by diagenesis. In fact, the unusually high abundances of *D. saipanensis* and *D. barbadiensis* are clearly a diagenetic artifact, since discoasters are one of the most solution-resistant forms (e.g., Raffi and De Bernardi, 2008). Strong dissolution is also indicated by the low abundance and poor preservation of the less resistant species such as *E. formosa* and by the high abundance of dissolved/fragmented placoliths (almost exclusively of *Dictyococcites*), consistently detected in both LM and SEM observations.

Dissolution is a complex phenomenon controlled by numerous factors, which can take place from the surface waters down through the water column, at the water-sediment interface, and even at considerable depths beneath the seafloor (e.g., Self-Trail and Seefelt, 2005). These factors may encompass, among others: variations in pH levels in pore waters, the mineral composition of the sediment, the existence of protective substrates surrounding coccoliths (e.g., fecal pellets, pores, pits), and the presence of bacteria in the seawater (Holcová and Scheiner, 2023). In addition to the previously mentioned processes, particularly concerning calcareous nannofossils, dissolution and fragmentation could also be influenced by decrease in accumulation rates and the consequent increase in their residence time at the sediment-water interface. During the pre-Eocene-Oligocene Transition (EOT) phase at Site 1209, low sedimentation rates and most likely a short hiatus (indicated by the simultaneous extinctions of rosette-shaped discoasters) were observed (Fig. 3). Our interpretation suggests that during this phase, the reduced sedimentation rates might have prolonged the residence time of nannofossils at the water-sediment interface and/or just below it, potentially contributing further to their alteration (dissolution and subsequent overgrowth). Moreover, it is worth noting that

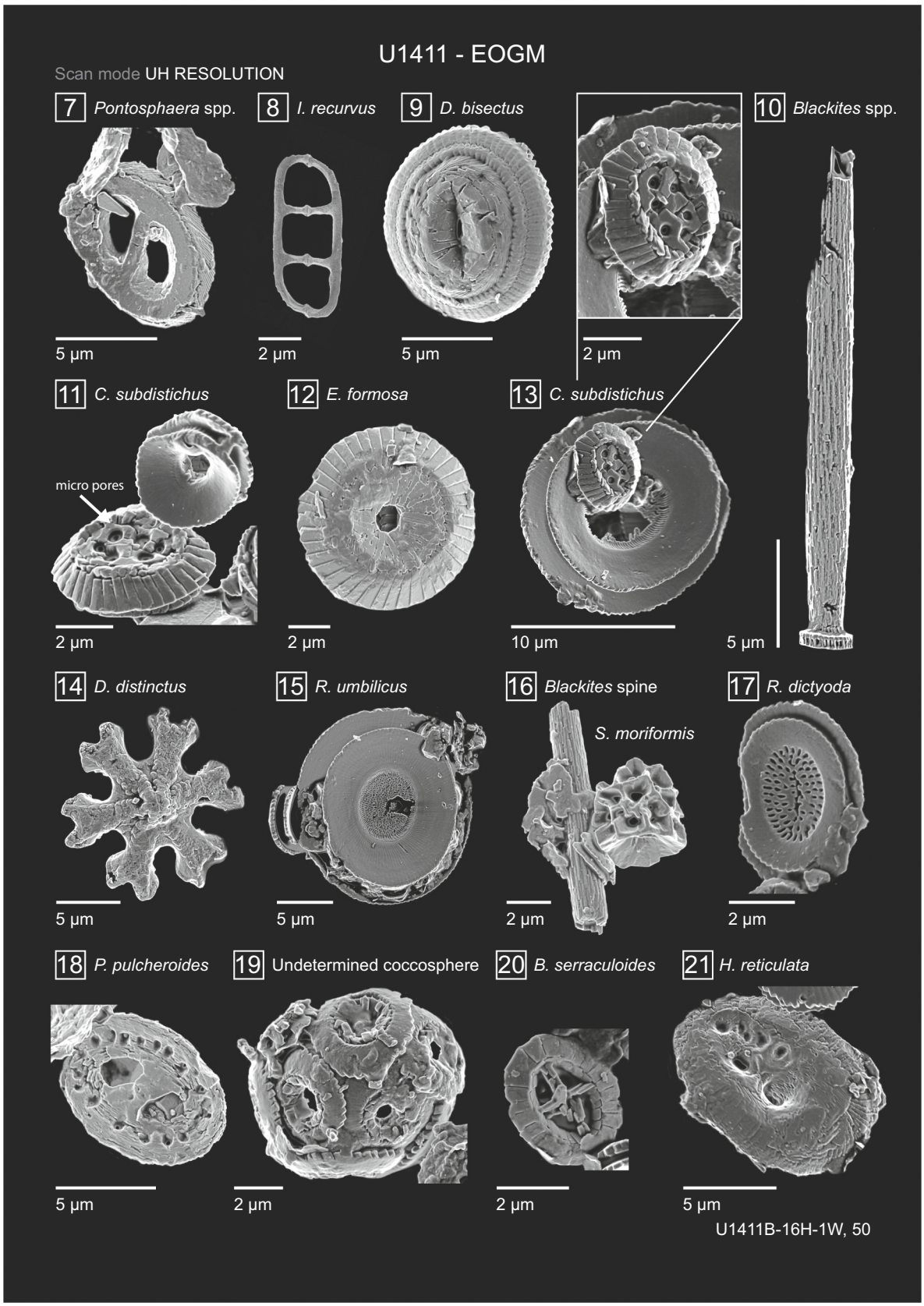

Fig. 12. (*continued*).

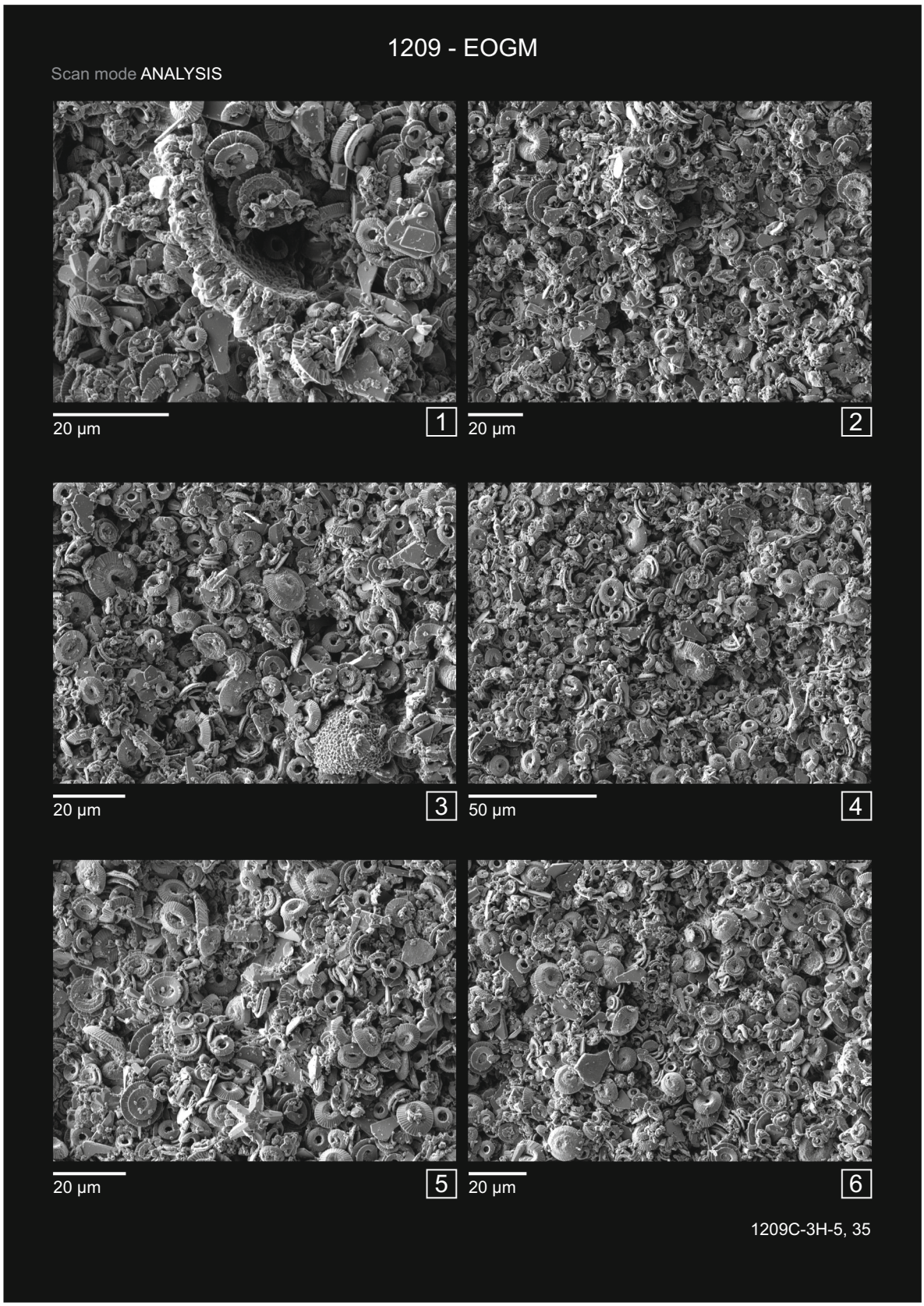

Fig. 13. Scanning electron photomicrographs showing the preservation of EOGM calcareous nannofossils from Site 1209 (Sample 1209-3H-5, 35 cm). Insets:
1–6 Analysis scan mode micrographs showing the assemblage constituents.
7 ***Sphenolithus moriformis***.
8 ***Hayella situliformis***.
9 ***Dictyococcites bisectus***.

10 ***Sphenolithus*** **spp**.
11 ***Reticulofenestra umbilicus*** lacking the perforate net in the central area.
12 ***Coccolithus pelagicus***.
13, 14 ***Ericsonia formosa***.
15 ***Discoaster tanii***.
16 Undetermined placolith (proximal).
17, 18 ***Bramletteius serraculoides*** lateral view (17) and along the c-axis orientation (18).
19 ***Dictyococcites*** **cf.** ***D. hesslandii***

reworking, while observed to some extent throughout the entire section (from 1 up to 3 n/mm^2), is notably more prominent during intervals of strong dissolution (E3, up to 8 n/mm^2) (Fig. 3, shaded pink bar). This observation can be readily explained by the fact that, coinciding with intense dissolution processes, only exceptionally robust and resistant taxa, such as *C. grandis, D. multiradiatus*, and *D.* cf. *D. robustus*, are reworked due to their ability to withstand the dissolution (Adelseck et al., 1973; Agnini et al., 2016).

During the Late Eocene Event (LEE), overgrowth is dominant, along with minor dissolution (E2). At Site 1209, there is no systematic increase in overgrowth with depth of burial, which agrees with preliminary shipboard observations (Bralower et al., 2005) but disagrees with other studies that document a general direct proportionality between increasing depth and overgrowth in homogeneous lithologies (Hill, 1975; Matter et al., 1975). Thus, preservation, in this case, partially results from the increasing depth but is mainly controlled by mechanisms related to pore fluids, possibly enhanced by the scarcity of clay minerals that is a typical trait of pelagic sediments (Bralower et al., 2002b). The increase in calcite overgrowth suggests a local basification of marine pore fluids and secondary precipitation during post-depositional processes.

Through the EOT interval, preservation tends to gradually improve, although overgrowth is still strongly present: as dissolution decreases, micro-sized calcite particles ("micarbs") and fragmentation also decrease.

In the EOGM, the preservation shows no major differences compared to the previous phase. The diagenetic process seems to reach stability that persists through the lower Oligocene interval. In summary, the low-diversity and poorly preserved nannofossil assemblage from Shatsky Rise is mainly the result of early diagenetic overprinting. Some taxa are more likely to be affected by diagenetic overgrowth, for instance *Discoaster*, *B. serraculoides*, *I. recurvus*, *Dictyococcites*, *S. radians* gr. and *S. predistentus*. Other coccoliths proved to be extremely solution-resistant, as the case of *S. intercalaris* probably due to its massive structure, and *H. stuliformis*, with strongly imbricated elements. Other taxa with delicate structures are instead more susceptible to differential dissolution, as is the case with the central area of *E. formosa* and the central nets of reticulofenestrids.

At ODP Site 1209, carbonate content is high and ranges between ~41 to 100%. This site represents a typical deep-sea section, commonly encountered studying the E-O transition, and characterized by pervasive overgrowth and/or dissolution due to diagenetic processes typically active in a carbonate-rich nannofossil ooze.

In contrast, the clay-rich nature of the drift sediments recovered at Hole U1411B has resulted in extraordinarily high species diversity and predominance of delicate central structures and small forms (Newsam, 2017).

Both Hole U1411B and Site 1209 share a similar paleodepth, with 2800 m and 2000 m, respectively. However, the main difference lies in their linear sedimentation rates (LSRs), with Hole U1411B averaging about ~2 cm/kyr, which is four times greater than at Site 1209. Additionally, there is a significant contrast in clay content, with the clay content being much higher at Site U1411 compared to Site 1209. Our comparative analysis indicates that the preservation state of coccoliths, at similar water depths, is enhanced in settings with high linear sedimentation rates (LSRs) and a high clay content because these factors act as protective substrates, effectively inhibiting diagenetic alterations.

4.3. Diagenetic effects on bulk isotopic data

Bulk sediment is composed of multiple, mostly biogenic, carbonate components (calcareous nannofossils, planktonic/benthic foraminifera, calcispheres and fragments). However, as recently underlined by Reghellin et al. (2015), calcareous nannofossils often dominate bulk marine carbonate in open ocean sediments, as in this case, carrying geochemical signals of mixed-layer conditions. Consequently, bulk stable isotopic composition ($\delta^{18}O$ and $\delta^{13}C$), coupled with carbonate content (%) have the potential to provide a valuable archive for paleoceanographic studies, as well as stratigraphic correlations. However, the successful application of bulk stable isotopes for accurate paleoceanographic reconstructions relies on the maintaining of the primary isotopic signal of deep-sea carbonates. For this reason, reliable paleoclimatic interpretations strongly depend on sediments that contain components (e.g., fossils) with well-preserved primary calcite. Despite this, paleoclimatologists often want to use and interpret data obtained from poorly to moderate preserved material. Overall, the preservation of coccoliths, which are one of the main constituent of the pelagic calcareous ooze, strongly relies on paleowater depth, because the undersaturation of seawater increases with pressure and decreasing temperature: as the depth of deposition increases, so does the rate of carbonate dissolution (Berger, 1974). So, shallow depositional sites tend to promote preservation in contrast to more deeper open-ocean sites (Berger, 1971; McIntyre and McIntyre, 1971; Johnson et al., 1977). ODP Site 1209 is well above the lysocline, and consequently the general poor preservation observed is primarily related to diagenetic processes taking place at water/sediment interface and/or in pore waters.

Our results indicate that, within the pre-EOT phase, precisely from 35.07 to 34.72 Ma, $\delta^{18}O$ values shift from a minimum of −0.54‰ to a maximum of 0.82‰; these values are not consistent with the long-term and short-term climate evolution in global oxygen isotope reference curves for the late Eocene (Fig. 5; Westerhold et al., 2020). This interval coincides with a high dissolution phase concomitant to moderate recrystallisation of secondary calcite of unknown isotopic values. The dissolution-precipitation reaction often takes place simultaneously (van der Lingen and Packham, 1975) and must have started before or soon after the burial. During this interval, both these processes contribute to high and low anomalous $\delta^{18}O$ values. However, no evidence of signal distortion was observed above this level, when comparing the $\delta^{18}O$ profiles from different Pacific Ocean sites (Fig. 5), despite overgrowth of coccoliths being recorded (Figs. 9, 11, 13). This supports the evidence gathered with single coccolith SIMS studies of the trace metal compositions from EOT successions in the equatorial Pacific, that found that primary nannofossil carbonate was robustly preserved, even beneath overgrowths (Prentice et al., 2014). The $\delta^{18}O$ bulk profile at Site 1209 closely parallels that from Site U1509 (Viganò et al., in prep.). Bulk $\delta^{18}O$ values at Site 1209 are slightly higher (mean $\delta^{18}O$ 0.56‰ ± 0.38‰) than those of associated bulk samples from well-preserved sediments (Site U1509, mean $\delta^{18}O$ 0.41‰ ± 0.21‰), but fall within quite close standard

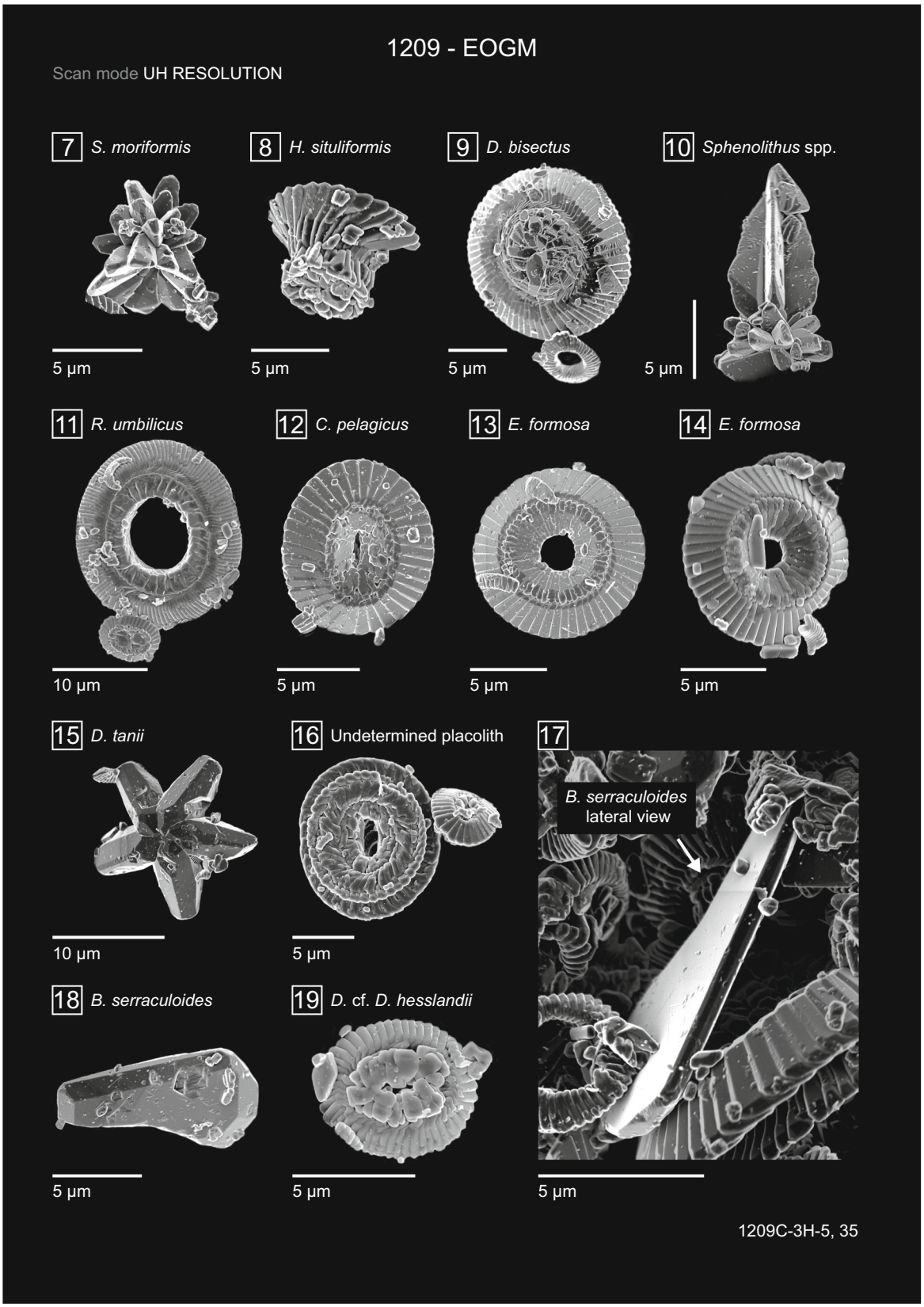

Fig. 13. (*continued*).

deviation ranges, indicating a negligible contribution of recrystallization in raising $\delta^{18}O$.

5. Conclusions

The semi-quantitative biostratigraphic analyses carried out at Sites 1209 and U1411, integrated with magnetostratigraphic and isotopic data, have provided independent age models for both sites and revealed additional potential biohorizons (e.g., Tc of *C. subdistichus* gr., the Bc of *S. predistentus* and *S. akropodus*, the Top of *I. recurvus*) that could be used to refine the resolution of the upper Eocene to lower Oligocene interval.

In this study we observed large inter-site differences in the preservation state of calcareous nannofossils implying very different diagenetic histories. At Hole U1411B, calcareous nannofossil assemblages are almost pristine and no significant alterations were found during the investigated phases. The presence of clay, very abundant during the pre-EOT and EOT, and the relatively low $CaCO_3$ (wt, %), has resulted in excellent preservation of taxa, including the most fragile and delicate forms. This contrasts with the results obtained from the pelagic carbonate-rich sediments of Shatsky Rise (ODP Site 1209), where dissolution and recrystallization were dominant in controlling the composition of nannofossil assemblage.

Dissolution and reprecipitation were extremely efficient in altering the original morphology of several taxa (e.g., *Discoaster*, *E. formosa*, *Dictyococcites*) as well as in completely dissolving other, normally common, but fragile EOT taxa (e.g., small reticulofenestrids), thus precluding any paleo-environmental interpretation.

The effects of diagenetic alteration occurred during the pre-EOT phase in the basal portion of the succession, severely altered the bulk stable isotopic data, resulting in extremely anomalous $\delta^{18}O$ values.

On the other hand, the geochemical signature recorded in the remaining part of the study interval, approximately started from 34.7 Ma, seems to be not compromised, although the effects of recrystallization on the nannofossil assemblage were severe during this phase. Thus, despite some diagenetic issues, we were able to recognize the primary global isotopic signature of the EOT. To conclude, while our result seems to suggest the maintenance of the primary EOT $\delta^{18}O$ signal even in a relatively poorly preserved carbonate-rich sediment, this outcome should be further tested over wide areas, in similar depositional settings.

Declaration of Competing Interest

The authors declare that they have no known competing financial interests or personal relationships that could have appeared to influence the work reported in this paper.

Data availability

Data will be made available on request.

Acknowledgements

The authors are grateful to the Integrated Ocean Drilling Program (IODP) for providing samples and data used in this study. The IODP is sponsored by the U.S. National Science Foundation (NSF) and participating countries under the management of Joint Oceanographic Institutions, Inc.

A. V. and C. A. were supported by University of Padova.

References

Adelseck, C.G., Geehan, G.W., Roth, P.H., 1973. Experimental evidence for the selective dissolution and overgrowth of calcareous nannofossils during diagenesis. Bull. Geol. Soc. Am. 84, 2755–2762.

Agnini, C., Fornaciari, E., Raffi, I., Catanzariti, R., Pälike, H., Backman, J., Rio, D., 2014. Biozonation and biochronology of Paleogene calcareous nannofossils from low and middle latitudes. Newsl. Stratigr. 47, 131–181.

Agnini, C., Fornaciari, E., Rio, D., Tateo, F., Backman, J., Giusberti, L., 2007. Responses of calcareous nannofossil assemblages, mineralogy and geochemistry to the environmental perturbations across the Paleocene/Eocene boundary in the venetian Pre-Alps. Mar. Micropaleontol. 63, 19–38.

Agnini, C., Spofforth, D.J.A., Dickens, G.R., Rio, D., Pälike, H., Backman, J., Muttoni, G., Dallanave, E., 2016. Stable isotope and calcareous nannofossil assemblage record of the late Paleocene and early Eocene (Cicogna section). Clim. Past 12, 883–909.

Backman, J., Shackleton, N.J., 1983. Quantitative biochronology of Pliocene and early Pleistocene calcareous nannofossils from the Atlantic, indian and Pacific oceans. Mar. Micropaleontol. 8, 141–170.

Bathurst, R.G.C., 1972. Carbonate sediments and diagenesis. In: Developements in Sedimentology, Vol. 12. Elsevier iii–xii, 1–658.

Berger, W.H., 1974. Deep-sea sedimentation. In: Burk, C.A., et al. (Eds.), The Geology of Continental Margins. Springer Science+Business Media New York, pp. 213–241.

Berger, W.H., 1971. Sedimentation of planktonic foraminifera. Mar. Geol. 11, 325–358.

Berggren, William, A., Kent, D.V., Swisher, C.C., Aubry, Marie-Pierre, 1995. A Revised Cenozoic geochronology and chronostratigraphy. In: Berggren, W., Kent, D.V., Aubry, M.-P., Hardenbol, J. (Eds.), Geochronology, Time Scales, and Global Stratigraphic Correlation: A Unified Temporal Framework for an Historical Geology. Special publication - Society of Economic Paleontologists and Mineralogists, pp. 129–212.

Birch, H.S., Coxall, H.K., Pearson, P.N., Kroon, D., Schmidt, D.N., 2016. Partial collapse of the marine carbon pump after the Cretaceous-Paleogene boundary. Geology 44, 287–290.

Bordiga, M., Henderiks, J., Tori, F., Monechi, S., Fenero, R., Legarda-Lisarri, A., Thomas, E., 2015. Microfossil evidence for trophic changes during the Eocene-Oligocene transition in the South Atlantic (ODP Site 1263, Walvis Ridge). Clim. Past 11, 1249–1270.

Bown, P.R., 2005. In: Cenozoic calcareous nannofossil biostratigraphy, ODP Leg 198 Site 1208 (Shatsky Rise, northwest Pacific Ocean). Proceedings of the Ocean Drilling Program, Scientific Results, 198: College Station, TX: Ocean Drilling Program 198, pp. 1–44.

Bown, P.R., Dunkley Jones, T., 2006. New Palaeogene calcareous nannofossil taxa from coastal Tanzania: Tanzania Drilling Project Sites 11 to 14. J. Nannoplankton Res. 28, 17–34.

Bown, P.R., Dunkley Jones, T., Lees, J.A., Randell, R.D., Mizzi, J.A., Pearson, P.N., Coxall, H.K., Young, J.R., Nicholas, C.J., Karega, A., Singano, J.M., Wade, B.S., 2008. A Paleogene calcareous microfossil Konservat-Lagerstätte from the Kilwa Group of coastal Tanzania. Geol. Soc. Am. Bull. 120, 3–12.

Bown, P.R., Gibbs, S.J., Sheward, R., O'Dea, S., Higgins, D., 2014. Searching for cells: the potential of fossil coccospheres in coccolithophore Searching for cells: the potential of fossil coccospheres in coccolithophore research. J. Nannoplankton Res. 34, 5–21.

Bown, P.R., Young, J.R., 1998. Techniques. In: Bown, P.R. (Ed.), Calcareous Nannofossil Biostratigraphy. Kluwer Academic Publishers, London, pp. 16–28.

Bralower, T.J., Premoli Silva, I., Malone, M.J., 2005. Data report: Paleocene-early Oligocene calcareous nannofossil biostratigraphy, ODP Leg 198 Sites 1209, 1210, and 1211 (Shatsky Rise, Pacific Ocean). In: Proceedings of the Ocean Drilling Program, Scientific Results, 198, College Station, TX (Ocean Drilling Program), pp. 1–15.

Bralower, T.J., Premoli Silva, I., Malone, M.J., 2002. Leg 198 Summary. In: Proceedings of the Ocean Drilling Program, Initial Reports Volume 198, College Station, TX (Ocean Drilling Program), pp. 1–148.

Bralower, T.J., Premoli Silva, I., Malone, M.J., Shipboard Scientific Party, 2002. Site 1209. In: Proceedings of the Ocean Drilling Program, Initial Reports Volume 198, College Station, TX (Ocean Drilling Program), pp. 1–102.

Burdige, D.J., 2007. Geochemistry of Marine Sediments. Princeton University Press.

Cappelli, C., Bown, P.R., Westerhold, T., Bohaty, S.M., De Riu, M., Lobba, V., Yamamoto, Y., Agnini, C., 2019. The early to middle Eocene transition: an integrated calcareous nannofossil and stable isotope record from the Northwest Atlantic Ocean (IODP Site U1410). Paleoceanogr. Paleoclimatol. 34, 1–18.

Cisneros-Lazaro, D., Adams, A., Guo, J., Bernard, S., Baumgartner, L.P., Daval, D., Baronnet, A., Grauby, O., Vennemann, T., Stolarski, J., Escrig, S., Meibom, A., 2022. Fast and pervasive diagenetic isotope exchange in foraminifera tests is species-dependent. Nat. Commun. 13, 1–11.

Coxall, H.K., D'Hondt, S., Zachos, J.C., 2006. Pelagic evolution and environmental recovery after the Cretaceous-Paleogene mass extinction. Geology 34, 297.

Coxall, H.K., Pearson, P.N., 2007. The Eocene-Oligocene Transition. In: Williams, M., Haywood, A.M., Gregory, J., Schmidt, D.N. (Eds.), Deep-Time Perspectives on Climate Change: Marrying the Signal from Computer Models and Biological Proxies, Micropaleontology Society Special Publication. Geological Society, London, pp. 351–387.

Coxall, H.K., Wilson, P.A., Pälike, H., Lear, C.H., Backman, J., 2005. Rapid stepwise onset of Antarctic glaciation and deeper calcite compensation in the Pacific Ocean. Nature 433, 53–57.

de Kaenel, E., Villa, G., 1996. Oligocene Miocene calcareous nannofossil biostratigraphy and paleoecology from the Iberia Abyssal plain. Proc. Ocean Drill. Program Sci. Results 149, 79–145.

Dunkley Jones, T., Bown, P.R., Pearson, P.N., Wade, B.S., Coxall, H.K., Lear, C.H., 2008. Major shifts in calcareous phytoplankton assemblages through the Eocene-Oligocene transition of Tanzania and their implications for low-latitude primary production. Paleoceanography 23, 1–14.

Fioroni, C., Villa, G., Persico, D., Jovane, L., 2015. Middle Eocene-lower Oligocene calcareous nannofossil biostratigraphy and paleoceanographic implications from Site 711 (equatorial Indian Ocean). Mar. Micropaleontol. 118, 50–62.
Fisher, A.G., Honjo, S., Garrison, R.E., 1967. Electron Micrographs of Limestones and their Nannofossils. Princeton University Press, Princeton, New Jersey.
Gradstein, F.M., Ogg, J.G., Schmitz, M.D., Ogg, G.M., 2020. Geological Time Scale 2020. Elsevier.
Hill, M.E., 1975. Selective dissolution of mid-cretaceous (Cenomanian) calcareous nannofossils. Micropaleontology 21, 227–235.
Holcová, K., Scheiner, F., 2023. An experimental study on post-mortem dissolution and overgrowth processes affecting coccolith assemblages: a rapid and complex process. Geobiology 21, 193–209.
Honjo, S., 1976. Coccoliths: production, transportation and sedimentation. Mar. Micropaleontol. 1, 65–79.
Hutchinson, D.K., Coxall, H.K., Lunt, D.J., Steinthorsdottir, M., de Boer, A.M., Baatsen, M., von der Heydt, A., Huber, M., Kennedy-Asser, A.T., Kunzmann, L., Ladant, J.B., Lear, C.H., Moraweck, K., Pearson, P.N., Piga, E., Pound, M.J., Salzmann, U., Scher, H.D., Sijp, W.P., Śliwińska, K.K., Wilson, P.A., Zhang, Z., 2021. The Eocene-Oligocene transition: a review of marine and terrestrial proxy data, models and model–data comparisons. Clim. Past 17, 269–315.
Jenkyns, H.C., 1980. Cretaceous anoxic events: from continents to oceans. J. Geol. Soc. 137, 171–188.
Johnson, T.C., Hamilton, E.L., Berger, W.H., 1977. Physical properties of calcareous ooze: Control by dissolution at depth. Mar. Geol. 24, 259–277.
Jones, A.P., Dunkley Jones, T., Coxall, H.K., Pearson, P.N., Nala, D., Hoggett, M., 2019. Low-Latitude Calcareous Nannofossil Response in the Indo-Pacific warm Pool across the Eocene-Oligocene transition of Java, Indonesia. Paleoceanogr. Paleoclimatol. 34, 1833–1847.
Liu, Z., Tuo, S., Zhao, Q., Cheng, X., Huang, W., 2004. Deep-water earliest Oligocene glacial maximum (EOGM) in South Atlantic. Chin. Sci. Bull. 49, 2190–2197.
Matter, A., Douglas, R.G., Perch-Nielsen, K., Larson, R.L., Moberly, R., Matter, A., Douglas, R.G., Perch-Nielsen, K., 1975. Fossil Preservation, Geochemistry, and Diagenesis, of Pelagic Carbonates from Shatsky Rise. In: Northwest Pacific, Initial Reports of the Deep Sea Drilling Project, p. 32.
McIntyre, A., McIntyre, R., 1971. Coccolith concentrations and differential solution in oceanic sediments. In: Funnel, B.M., Riedel, W.R. (Eds.), The Micropalaeontology of the Oceans. Cambridge University Press, pp. 253–261.
Miller, K.G., Wright, J.D., Fairbanks, R.G., 1991. Unlocking the Ice House: Oligocene-Miocene oxygen isotopes, eustasy, and margin erosion. J.Geophys.Res. Solid Earth 96, 6829–6848.
Morse, J.W., 2003. Formation and diagenesis of carbonate sediments. Treat. Geochem. 7–9, 67–85.
Newsam, C., 2017. Calcareous nannoplankton evolution and the Paleogene greenhouse to icehouse climate-mode transition. University College London (UCL). Doctoral thesis.
Norris, R.D., Wilson, P.A., Blum, P., Fehr, A., Agnini, C., Bornemann, A., Boulila, S., Bown, P.R., Cournede, C., Friedrich, O., Ghosh, A.K., Hollis, C.J., Hull, P.M., Jo, K., Junium, C.K., Kaneko, M., Liebrand, D., Lippert, P.C., Liu, Z., Matsui, H., Moriya, K., Nishi, H., Opdyke, B.N., Penman, D.E., Romans, B.W., Scher, H.D., Sexton, P., Takagi, H., Turner, S.K., Whiteside, J.H., Yamaguchi, T., Yamamoto, Y., 2014. In: Site U1411. Proceedings of the Integrated Ocean Drilling Program 342, p. 76.
Norris, R.D., Wilson, P.A., Blum, P., Fehr, A., Agnini, C., Bornemann, A., Boulila, S., Bown, P.R., Cournede, C., Friedrich, O., Kumar Ghosh, A., Hollis, C.J., Hull, P.M., Jo, K., Junium, C.K., Kaneko, M., Liebrand, D., Lippert, P.C., Liu, Z., Matsui, H., Moriya, K., Nishi, H., Opdyke, B.N., Penman, D., Romans, B., Scher, H.D., Sexton, P., Takagi, H., Kirtland Turner, S., Whiteside, J.H., Yamaguchi, T., Yamamoto, Y., Scully, C., Brinkhuis, D.F., Flemings, P.B., Iturrino, G.J., Meissner, E., Pettigrew, T.L., Polito, P.J., Aduddell, R., Barnes, H., Beck, J., Bertoli, M., Bloxom, T., Cannon, M., Claassen, E., Cobine, T., Davis, R., Fulton, T., Gustafson, T., Herrmann, S., Meiring, M., Midgley, S., Moortgat, E., Morgan, A., Peng, C., Prinz, S., Swain, K., Vasilyeva, Y., Weymer, B., James Zhao, H., 2012. Paleogene newfoundland sediment drifts. Integrated Ocean Drilling Program, Expedition 342, Preliminary Report 1–263.
Pälike, H., Lyle, M.W., Nishi, H., Raffi, I., Ridgwell, A., Gamage, K., Klaus, A., Acton, G., Anderson, L., Backman, J., Baldauf, J., Beltran, C., Bohaty, S.M., Bown, P.R., Busch, W., Channell, J.E.T., Chun, C.O.J., Delaney, M.L., Dewangan, P., Dunkley Jones, T., Edgar, K.M., Evans, H., Fitch, P., Foster, G.L., Gussone, N., Hasegawa, H., Hathorne, E.C., Hayashi, H., Herrle, J.O., Holbourn, A.E., Hovan, S., Hyeong, K., Iijima, K., Ito, T., Kamikuri, S.I., Kimoto, K., Kuroda, J., Leon-Rodriguez, L., Malinverno, A., Moore, T.C., Murphy, B.H., Murphy, D.P., Nakamura, H., Ogane, K., Ohneiser, C., Richter, C., Robinson, R., Rohling, E.J., Romero, O., Sawada, K., Scher, H.D., Schneider, L., Sluijs, A., Takata, H., Tian, J., Tsujimoto, A., Wade, B.S., Westerhold, T., Wilkens, R., Williams, T., Wilson, P.A., Yamamoto, Y., Yamamoto, S., Yamazaki, T., Zeebe, R.E., 2012. A Cenozoic record of the equatorial Pacific carbonate compensation depth. Nature 488, 609–614.
Pearson, P.N., Ditchfield, P.W., Singano, J., Harcourt-Brown, K.G., Nicholas, C.J., Olsson, R.K., Shackleton, N.J., Hall, M.A., 2001. Warm tropical sea surface temperatures in the late cretaceous and Eocene epochs. Nature 413, 481–487.
Pearson, P.N., McMillan, I.K., Wade, B.S., Dunkley Jones, T., Coxall, H.K., Bown, P.R., Lear, C.H., 2008. Extinction and environmental change across the Eocene-Oligocene boundary in Tanzania. Geology 36, 179–182.
Perch-Nielsen, K., 1979. Calcareous nannofossils from the cretaceous between the North Sea and the Mediterranean. Aspekte der Kreide Europas. IUGS Series A 6, 223–272.
Persico, D., Villa, G., 2004. Eocene-Oligocene calcareous nannofossils from Maud rise and Kerguelen Plateau (Antarctica): Paleoecological and paleoceanographic implications. Mar. Micropaleontol. 52, 153–179.
Premoli Silva, I., Jenkins, D.G., 1993. Decision on the Eocene-Oligocene boundary stratotype. Episodes 16, 379–382.
Prentice, K., Jones, T.D., Lees, J., Young, J., Bown, P., Langer, G., Fearn, S., 2014. Trace metal (Mg/Ca and Sr/Ca) analyses of single coccoliths by secondary Ion Mass Spectrometry. Geochim. Cosmochim. Acta 146, 90–106.
Raffi, I., De Bernardi, B., 2008. Response of calcareous nannofossils to the Paleocene-Eocene thermal Maximum: Observations on composition, preservation and calcification in sediments from ODP Site 1263 (Walvis Ridge - SW Atlantic). Mar. Micropaleontol. 69, 119–138.
Reghellin, D., Coxall, H.K., Dickens, G.R., Backman, J., 2015. Carbon and oxygen isotopes of bulk carbonate in sediment deposited beneath the eastern equatorial Pacific over the last 8 million years. Paleoceanography 30, 1261–1286.
Roth, P.H., 1983. Jurassic and Lower Cretaceous calcareous nannofossils in the western North Atlantic (Site 534): biostratigraphy, preservation, and some observations on biogeography and paleoceanography. Initial reports DSDP, Leg 76, Norfolk to Fort Lauderdale 587–621.
Roth, P.H., Thierstein, H., 1972. Calcareous Nannoplankton: Leg 14 of the Deep Sea Drilling Project. Initial Reports of the Deep Sea Drilling Project, 14.
Roth, P.R., 1978. In: Cretaceous Nannoplankton Biostratigraphy and Oceanography of the Northwestern Atlantic Ocean. Initial Reports of the Deep Sea Drilling Project, p. 44.
Schlanger, S., Jenkyns, H., 1976. Cretaceous oceanic anoxic events: causes and consequences. Geol. Mijnb. 55, 179–184.
Schneider, L.J., Bralower, T.J., Kump, L.R., 2011. Response of nannoplankton to early Eocene Ocean destratification. Palaeogeogr. Palaeoclimatol. Palaeoecol. 310, 152–162.
Self-Trail, J.M., Seefelt, E.L., 2005. Rapid dissolution of calcareous nannofossils: a case study from freshly cored sediments of the South-Eastern Atlantic Coastal Plain. J. Nannoplankton Res. 27, 149–157.
Spofforth, D.J.A., Agnini, C., Pälike, H., Rio, D., Fornaciari, E., Giusberti, L., Luciani, V., Lanci, L., Muttoni, G., 2010. Organic carbon burial following the middle Eocene climatic optimum in the central western Tethys. Paleoceanography 25, PA3210.
Staudigel, P.T., Swart, P.K., 2019. A diagenetic origin for isotopic variability of sediments deposited on the margin of Great Bahama Bank, insights from clumped isotopes. Geochim. Cosmochim. Acta 258, 97–119.
Toffanin, F., Agnini, C., Rio, D., Acton, G., Westerhold, T., 2013. Middle Eocene to early Oligocene calcareous nannofossil biostratigraphy at IODP Site U1333 (equatorial Pacific). Micropaleontology 69–82.
van der Lingen, G.J., Packham, G.H., 1975. Relationships between diagenesis and physical properties of biogenic sediments of the Ontong- Java Plateau (Sites 288 and 289, Deep Sea Drilling Project). Initial Rep. Deep Sea Drill. Proj. 30, 443–481.
Viganò, A., Coxall, H.K., Holmström, M., Vinco, M., Lear, C.H., Agnini, C., 2023. Calcareous nannofossils across the Eocene-Oligocene transition at Site 756 (Ninetyeast Ridge, Indian Ocean): implications for biostratigraphy and paleoceanographic clues. Newsl. Stratigr. 56, 187–223.
Viganò, A., Dallanave, E., Alegret, L., Westerhold, T., Sutherland, R., Dickens, G.R., Newsam, C., Agnini, C., in press. Calcareous nannofossil biostratigraphy and biochronology across the Eocene-Oligocene transition: the record at IODP Site U1509 (Tasman Sea) and a global overview. Newslett.Stratigr. 57.
Villa, G., Fioroni, C., Pea, L., Bohaty, S.M., Persico, D., 2008. Middle Eocene-late Oligocene climate variability: Calcareous nannofossil response at Kerguelen Plateau, Site 748. Mar. Micropaleontol. 69, 173–192.
Villa, G., Fioroni, C., Persico, D., Roberts, A.P., Florindo, F., 2014. Middle Eocene to late Oligocene Antarctic glaciation/deglaciation and Southern Ocean productivity. Paleoceanography 29, 223–237.
Villa, G., Florindo, F., Persico, D., Lurcock, P., de Martini, A.P., Jovane, L., Fioroni, C., 2021. Integrated calcareous nannofossil and magnetostratigraphic record of ODP Site 709: Middle Eocene to late Oligocene paleoclimate and paleoceanography of the Equatorial Indian Ocean. Mar. Micropaleontol. 169, 102051.
Westerhold, T., Marwan, N., Drury, A.J., Liebrand, D., Agnini, C., Anagnostou, E., Barnet, J.S.K., Bohaty, S.M., De Vleeschouwer, D., Florindo, F., Frederichs, T., Hodell, D.A., Holbourn, A.E., Kroon, D., Lauretano, V., Littler, K., Lourens, L.J., Lyle, M., Pälike, H., Röhl, U., Tian, J., Wilkens, R.H., Wilson, P.A., Zachos, J.C., 2020. An astronomically dated record of Earth's climate and its predictability over the last 66 million years. Science 369, 1383–1388.
Westerhold, T., Röhl, U., 2006. Data report: revised composite depth records for Shatsky Rise Sites 1209, 1210, and 1211. In: Bralower, T.J., Premoli Silva, I., Malone, M.J. (Eds.), Proceedings of the Ocean Drilling Program, Scientific Results Volume 198: College Station, TX (Ocean Drilling Program, pp. 1–26.
Westerhold, T., Röhl, U., Pälike, H., Wilkens, R., Wilson, P.A., Acton, G., 2014. Orbitally tuned timescale and astronomical forcing in the middle Eocene to early Oligocene. Clim. Past 10, 955–973.
Zachos, J.C., Dickens, G.R., Zeebe, R.E., 2008. An early Cenozoic perspective on greenhouse warming and carbon-cycle dynamics. Nature 451, 279–283.
Zachos, J.C., Pagani, M., Sloan, L., Thomas, E., Billups, K., 2001. Trends, Global Rhythms, and Aberrations in Global climate 65 Ma to present. Science 292, 686–693.
Zachos, J.C., Quinn, T.M., Salamy, K.A., 1996. High-resolution (104 years) deep-sea foraminiferal stable isotope records of the Eocene-Oligocene climate transition. Paleoceanography 11, 251–266.